

Excited-state hydroxyl maser catalogue from the methanol multibeam survey – I. Positions and Variability

A. Avison,^{1,2} [★], L.J. Quinn,^{2,3}, G.A. Fuller,^{1,2}, J.L. Caswell⁴ [†], J.A. Green,^{4,5}, S.L. Breen⁴, S.P. Ellingsen⁶, M.D. Gray,², M. Pestalozzi,⁷, M. A. Thompson⁸ and M. A. Voronkov⁴

¹UK ALMA Regional Centre Node

²Jodrell Bank Centre for Astrophysics, Alan Turing Building, School of Physics and Astronomy, The University of Manchester, Manchester, M13 9PL, UK

³Bury College, Millennium Centre, Market Street, Bury BL9 0DB, UK

⁴CSIRO Astronomy and Space Science, Australia Telescope National Facility, PO Box 76, Epping, NSW 2121, Australia

⁵SKA Organization, Jodrell Bank Observatory, Lower Withington, Macclesfield, Cheshire SK11 9DL, UK

⁶School of Physical Sciences, University of Tasmania, Private Bag 37, Hobart, TAS 7001, Australia

⁷Istituto di Astrofisica e Planetologia Spaziali IAPS - INAF, via del Fosso del cavaliere 100, I-00133 Roma, Italy

⁸Centre for Astrophysics Research, Science and Technology Research Institute, University of Hertfordshire, College Lane, Hatfield AL10 9AB

Released 2016 XXXX XX

ABSTRACT

We present the results of the first complete unbiased survey of the Galactic Plane for 6035-MHz excited-state hydroxyl masers undertaken as part of the Methanol Multibeam Survey. These observations cover the Galactic longitude ranges $186^\circ < l < 60^\circ$ including the Galactic Centre. We report the detection of 127 excited-state hydroxyl masers within the survey region, 47 being new sources. The positions of new detections were determined from interferometric observations with the Australia Telescope Compact Array. We discuss the association of 6035-MHz masers in our survey with the 6668-MHz masers from the MMB Survey, finding 37 likely CH₃OH–ex-OH maser pairs with physical separations of ≤ 0.03 pc and 55 pairings separated by ≤ 0.1 pc. Using these we calculate for the first time an excited-state hydroxyl maser life time of between 3.3×10^3 and 8.3×10^3 years. We also discuss the variability of the 6035-MHz masers and detection rates of counterpart 6030-MHz excited-state hydroxyl masers (28% of our sample having detection at both frequencies).

Key words: masers – surveys – stars: formation – ISM: molecules – Galaxy: structure

1 INTRODUCTION

The Methanol Multibeam (MMB) survey is an unbiased Galactic plane survey searching for the 6668-MHz methanol maser line (Green et al. 2009). The MMB survey region covers the whole southern portion of the Galactic plane (longitudes $186^\circ < l < 60^\circ$, latitude $|b| \leq 2^\circ$).

The 6668-MHz methanol maser transition is uniquely associated with high-mass star formation (Minier et al. 2003; Xu et al. 2008; Breen et al. 2013) making it a clear signpost of regions of high-mass star formation and their distribution throughout the Milky Way. Ground-state and excited-state hydroxyl (hereafter ex-OH) maser transitions are often associated with the 6668-MHz methanol maser

(e.g. Caswell 1997, 1998). First observed in the late 1960s and early 1970s (e.g. Yen et al. 1969; Rydbeck et al. 1970) the $^2\Pi_{3/2} J = 5/2, F = 3 - 3$ ex-OH maser transition at 6035-MHz and the nearby, often weaker, 6030-MHz maser line ($^2\Pi_{3/2} J = 5/2, F = 2 - 2$) have been extensively studied with multiple targeted surveys, usually toward other maser species (e.g. 6668-MHz CH₃OH or ground-state OH, see Knowles et al. 1976; Caswell & Vaile 1995; Baudry et al. 1997; Caswell 1997, 2001). The ex-OH maser transitions are primarily observed toward star forming regions, with only two known examples observed toward evolved stars (Vy 2-2 and K 3-35, see Desmurs et al. 2010) making ex-OH masers in evolved stars extremely rare and a potentially transient phenomenon (Richards 2012). These sources are not present in this current work as both exist at Galactic latitudes outside of the MMB survey range.

When observed in association with the 6668-MHz

[★] Email: adam.avison@manchester.ac.uk

[†] Deceased 2015 January 14.

CH₃OH maser, the rarer ex-OH maser gives important additional information on the environment of the star forming region it inhabits. This maser transition appears to exist in pre-ionising high-mass protostellar objects as well as sources with ultra compact HII regions (Fish 2007, and references therein).

Ex-OH masers are predominantly radiatively pumped requiring a nearby source of infrared emission at wavelengths of the order ~ 30 – $120\mu\text{m}$ to generate the population inversion, (e.g. Cesaroni & Walmsley 1991; Gray et al. 1992; Gray 2001). Figure 1 shows rotational energy level diagram for both ground state and ex-OH transitions. Models of maser pumping by Cragg et al. (2002) find that both the 6030 and 6035-MHz transitions occur in zones of low gas temperatures ($T_k < 70\text{K}$) and high densities (up to $n_H = 10^{8.5}\text{cm}^{-3}$), covering a parameter space coincident with, but not identical to, both the 6668-MHz CH₃OH and ground-state OH (1612, 1665, 1667, 1720-MHz) masers (see also Gray et al. 1992). As such, coincident detection of multiple maser species can place constraints on the environment of a high-mass star forming region (e.g. Cragg et al. 2001; Sutton et al. 2001, for methanol). The ex-OH maser also provides important information about the magnetic fields in its local environment as OH has a relatively large Lande g-factor resulting in a significant Zeeman splitting of the maser lines (Fish 2007, and references therein).

In this paper we present the results from a survey for the 6035-MHz line of ex-OH carried out in parallel with the MMB survey. We present high signal-to-noise spectra at both 6035-MHz and 6030-MHz (the latter from targeted follow-up observations) for all sources and accurate interferometric positions for the newly detected masers, as well as discussing ex-OH maser source variability and association with 6668-MHz CH₃OH maser counterparts. In a companion paper we will explore the results of the survey in relation to the magnetic fields probed by the masers (Avison et al. *in prep*).

2 METHANOL MULTIBEAM SURVEY PARAMETERS AND EQUIPMENT

The full details of the techniques used by the MMB survey are presented in Green et al. (2009), therefore here we present only a summary of those points relevant to the ex-OH observations. The MMB survey was conducted as a blind survey using a custom built seven-beam receiver on the Parkes Radio Telescope. Using the receiver's 1-GHz bandwidth both the 6668-MHz CH₃OH line and the 6035-MHz ex-OH lines were surveyed simultaneously, to a typical RMS noise level of 0.17Jy (Green et al. 2009). The Parkes data included both Left-hand (LHCP) and Right-hand (RHCP) circular polarisation data.

Any new ex-OH detections or sources without previous high-resolution positions were then followed up with the Australia Telescope Compact Array (ATCA) to acquire a position (to within $\sim 0.4''$). Finally, to obtain high signal-to-noise spectra of these sources, they were observed again at Parkes using the ATCA position with an observing setup termed 'MX' (see Green et al. 2009). 'MX' observations at 6030-MHz were also obtained at positions of 6035-MHz emission to detect potential counterpart ex-OH masers at this

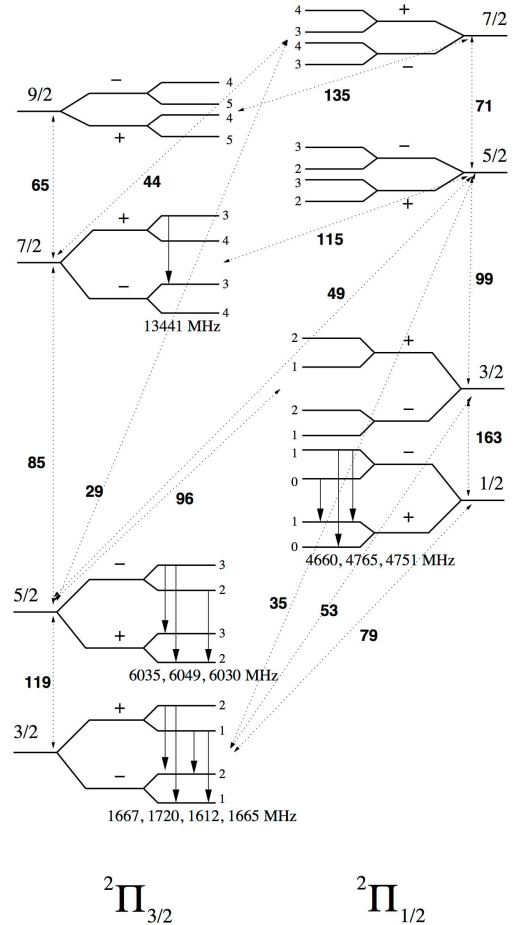


Figure 1. Rotational energy level diagram of OH up to $J = 9/2$. The level are split in to the left-hand $2\Pi_{3/2}$ and right-hand $2\Pi_{1/2}$ ladders by spin-orbit coupling. Each rotational level is split first into halves of opposite parity and then again by hyperfine splitting. The frequencies in MHz of emission are shown for various transitions below solid arrows for each J level. The values in bold next to dotted arrows give approximate wavelengths in microns. Figure and caption adapted from Gray (2012).

frequency. The typical RMS noises in the MX observations at 6035-MHz and 6030-MHz are 0.10Jy and 0.11Jy respectively.

2.1 Ex-OH ATCA observations

The positioning observations of forty-seven new ex-OH sources were made with ATCA in January 2009 over three days. Observations were conducted with the ATCA in the 6C configuration (maximum baseline 6.0km). The observations were made centred on the ex-OH 6035-MHz transition, with 2048 channels over a bandwidth of 4-MHz. The data were flux density and bandpass calibrated using the ATCA standard sources PKS B1934-638 and PKS B1921-293 respectively. Phase calibration was interleaved between on source observations of three to four maser sources which were close in position and velocity, using a calibration source local (typical offset $< 10^\circ$) to that area of sky.

Further ATCA observations were taken in October 2013

and February 2014 to complete the source positioning for new sources. These observing runs were each taken in blocks over one (Oct. 2013) and two days (Feb. 2014) in the H214 and 6D configurations (maximum baselines 274m and 6.0km respectively). They focused on the more northerly sources from the MMB survey. The CABB correlator system (Wilson et al. 2011) had replaced the correlator system used in the 2009 observations, the new observing setup providing 10,240 channels over a 5.0MHz bandwidth (giving 0.488 kHz channels). These observations provided full Stokes polarisation (XX, YY, XY, YX) and also included observations of the 6030-MHz line. For the Oct 2013 observations in the H214 array configuration antenna 6 (at 6.0km) was excluded from the data reduction meaning these data were taken with five antennas leading to higher RMS values. The positional accuracy of all ATCA observations for the MMB survey is approximately $0.4''$ (Caswell et al. 2010).

For all the ATCA observing epochs data reduction was conducted using the MIRIAD software package following standard ATNF reduction strategies for either pre- or post-CABB data.

3 SURVEY RESULTS

A total of 127 6035-MHz and 32 6030-MHz ex-OH masers are found within the MMB survey region, Galactic longitudes $186^\circ < l < 60^\circ$ and latitudes $|b| \leq 2^\circ$. We present in Table 1 the properties of the ex-OH masers found within this survey. Column 1 gives the source name defined as the source position in Galactic coordinates (rounded at the third decimal point) prefixed with MMBOH-G, columns 2 and 3 the J2000 Right Ascension and Declination co-ordinates. Column 4 the maser transition frequency, column 5 the literature or observational position reference for the RA and Dec. Columns 6, 7 and 8 give the maser peak flux density, peak velocity and a guideline velocity range from the Parkes MX of the LHCP maser emission, with columns 9, 10 and 11 the same for RHCP. The exceptions being sources *49.046–0.290* and *326.447–0.749* for which the Stokes I values from the ATCA data are presented in columns 6, 7 and 8 in italics.

Figure 11 shows the Parkes MX spectra for each ex-OH maser with the exception of sources *49.046–0.290* and *326.447–0.749* for which the Stokes I spectra from ATCA is used as these sources are not present in the nearest Parkes MX. The full version of this figure is available in the online version only.

Finally, there remains one ex-OH maser, *189.030+0.783* clearly present in the Parkes MX data but for which we have been unable to attain an ATCA position. This source is at high positive declination where the beam of the ATCA becomes elongated and positioning becomes difficult. This source is included in Table 1, and Figures 3 and 11 but is not included in any analysis beyond §4.2.4.

3.1 Remarks on sites of ex-OH maser emission

Here we provide additional information to that given in Table 1 on each of the 47 newly detected ex-OH sources, or those which have changed significantly since their last published observation. This additional information primarily focuses on association with 6030-MHz emission from the MMB

MX observations and any nearby MMB CH₃OH source. We also note if there are previous detections at 1665-MHz OH masers and then include any further comments. It should be noted that many of the new 6035-MHz detections are low flux density sources and as such there are only a small number of corresponding 6030-MHz detections (see §4.3 for these sources).

For new detections we systematically comment on the nearest detections in the Bolocam Galactic Plane Survey (BGPS; Rosolowsky et al. 2010; Aguirre et al. 2011) and the APEX Telescope Large Area Survey of the GALaxy (ATLASGAL, with sources prefixed AGAL; Schuller et al. 2009; Contreras et al. 2013; Urquhart et al. 2014) data. Both surveys trace dense clumps and cores in the mm/sub-mm indicative of regions of star formation which may be associated with the ex-OH in our sample. The BGPS covers a region of the Galactic plane from $349.5^\circ \leq l \leq 90.5^\circ$, $|b| \leq 0.5^\circ$; with the latitude range extended to $|b| \leq 1.5^\circ$ in some regions see Aguirre et al. 2011 at 1.1mm with an effective resolution of $33''$ with ATLASGAL covering a region of $280^\circ \leq l \leq 60^\circ$, $-2^\circ < b < 1^\circ$ (see Urquhart et al. 2014) at $870\mu\text{m}$ with a beam full width half-maximum of $19.2''$. We extend our search for nearby BGPS or ATLASGAL sources out to $30''$, approximately the resolution of BGPS (Schuller et al. 2009) and the median clumps size reported by Urquhart et al. (2014) for ATLASGAL. Additionally, we include the name of the nearest infrared to radio wavelength continuum source or star formation tracer to our ex-OH detection up to an angular separation of $5.0''$ equivalent to 0.1pc, the typical size of a star forming core at the fiducial distance to a high-mass star forming region of 5kpc.

For brevity some references to previous OH (both excited and ground-state) detection are abbreviated, these are as follows: FC89 is Forster & Caswell (1989) (1665-MHz, reported RMS noise $\sim 0.1\text{Jy}$), CV95 is Caswell & Vaile (1995) (6035-MHz, typical detection limit $\sim 0.3\text{Jy}$), C98 is Caswell (1998) (1665/7-MHz, detection $\sim 0.16\text{Jy}$), A00 is Argon et al. (2000) (1665/7-MHz, detection limit 0.9-2.7Jy) and C03 is Caswell (2003) (6035/0-MHz, reported RMS noise $\sim 0.03\text{--}0.05\text{Jy}$). Finally ‘ND’ stands for new detection, to differentiate them from known sources with additional comments.

4.682+0.278: ND, position from ATCA-2009 data. No 1665-MHz from C98. No 6030-MHz detection. BGPS G004.681+00.277 mm source within $3.9''$ (Rosolowsky et al. 2010) and AGAL 004.681+00.277 sub-mm source within $4.16''$. The nearest MMB CH₃OH maser, G04.676+0.276, is offset by an angular distance of $21.3''$.

6.882+0.094: ND, position from ATCA-2009 data. 6030-MHz detection in MMB MX both hands of polarisation. No counterpart 1665-MHz in C98, and a MMB CH₃OH maser, G06.881+0.093, nearby at $4.8''$ separation. No other radio/mm source within $5''$. (The source BGPS G006.885+00.091 source is at a distance of $6''$ and no ATLASGAL source is reported nearby).

8.352+0.478: ND, Positions from ATCA-2013 data. No known 1665-MHz or 6030-MHz counterparts. No radio/mm source within $5''$. This source is one of the ‘isolated’ ex-OH sources discussed in §4.4.4. No mm/sub-mm sources

are detected nearby by ATLASGAL or BGPS.

9.620+0.194 and 9.622+0.196: NDs, Positions from ATCA-2009 data, the pair are separated by $12.0''$. Each target has a 1665-MHz maser detected in C98, with a single detection at this site at 1665-MHz from FC89. No 6030-MHz detection from either source. These sources are small angular distances from the 6668-MHz maser pair *G09.619+0.193 and G09.621+0.196* (offsets $5.23''$ and $4.75''$) respectively. The 6668-MHz maser *G09.621+0.1–96* is the brightest methanol maser detected in the MMB survey with a peak flux density of 5239.85Jy (Green et al. 2010), whereas the 6035-MHz peak flux density from the ATCA-2009 data is 0.2Jy and from the MMB MX data $0.24/0.25\text{Jy}$ (LHCP/RHCP, respectively). The methanol maser is also known to periodically vary on timescales of 244 days (van der Walt et al. 2009). *9.620+0.194* is coincident with BGPS G009.620+00.194 (within our positional uncertainties) and is likely associated with AGAL 009.621+00.194 (offset $\sim 4.1''$), whilst *9.622+0.196* sits at greater separation from both these sources at $12.2''$ and $9.6''$ respectively.

10.322–0.258: ND, Position from ATCA-2009 data. Nearby is the radio source GPSR5 10.322–0.259 source ($2.63''$) (Becker et al. 1994) and an MMB CH_3OH maser, G10.320–0.259, at an offset of $4.70''$. At greater separation lie AGAL 010.321–00.257 and BGPS G010.320–00.258 at $4.5''$ and $7.0''$ respectively.

10.960+0.022: ND, Positions from ATCA-2013 data. No 6030-MHz detection in the MMB MX data nor a 1665-MHz detection in FC89, C98 or A00. The MMB CH_3OH maser source G10.958+0.022, is offset from this position by $7.1''$. Nearby mm/sub-mm cores are BGPS G010.959+00.020 (offset at $7.0''$) and AGAL 010.957+00.022 (offset at $11.6''$).

12.681–0.182: 1665-MHz maser seen in FC89, C98 and A00. ND from ATCA-2009. No 6030-MHz source detected in MX data. Within the W33 star-forming region. At an offset of $2.9''$ is the CH_3OH maser G12.681–0.182. BGPS G012.681–00.182 is offset at angular separation of $0.5''$ and AGAL 012.679–0.181 is offset by $\sim 9.2''$.

18.460–0.005: ND, Position from ATCA-2009. Outside of C98 range, no detections of 1665-MHz in FC89. No 6030-MHz source detected in MX data. Offset from Compact / UC HII region by $3.89''$ from e.g. Walsh et al. (1998) and the MMB CH_3OH maser, G18.460–0.004, by $1.6''$. Nearby are the dense mm/sub-mm cores of BGPS G018.462–00.002 at $12.7''$ and AGAL 018.461–00.002 at $9.8''$.

18.836–0.299: ND, position from ATCA-2009 data. Outside of C98 range, no detections of 1665-MHz in FC89. No 6030-MHz source detected in MMB MX data. The nearest MMB CH_3OH maser is G18.834–0.300 at an offset of $7.2''$. There are mm/sub-mm detections made by both BGPS and ATLASGAL with sources AGAL 018.833–00.301 and BGPS G018.834–00.299 offset from the maser peak by $10.6''$ and $5.1''$ respectively.

19.752–0.191: ND, positioning from the MMB ‘piggy-

back’ data (see Green et al. 2009 and Ellingsen et al. in prep.). 6030-MHz data unavailable for this source. This source is an ‘isolated’ ex-OH sources (discussed in §4.4.4) with no MMB CH_3OH detection within $>200''$ and the nearest BGPS and ATLASGAL detections over an arcminute away.

24.147–0.010: ND, position from ATCA-2009 data. No detection FC89 at 1665-MHz. Non detection of 6030-MHz in the MMB MX data. MMB CH_3OH maser source G24.148–0.009 is offset for this source position by $3.5''$. Nearby sub-mm detection of AGAL 024.148–00.009 (offset $4.1''$), whilst the nearest BGPS sources is G024.154–00.008 offset by $24.0''$.

25.509–0.060: ND, position from ATCA-2009 data. No detection FC89 at 1665-MHz nor a 6030-MHz source in MMB MX data. This source is an ‘isolated’ ex-OH sources (discussed in §4.4.4) with no MMB CH_3OH detection within $>400''$. No radio/mm sources within $5''$. There are no BGPS or ATLASGAL sources within 2 arcminutes.

25.648+1.050: ND, position from ATCA-2013. No 1665- or 6030-MHz counterpart. No mm- or radio source within $5''$. The MMB CH_3OH maser G25.650+1.049 is offset by $5.8''$. AGAL 025.649+01.051 is the nearest sub-mm detection at an angular offset of $3.9''$, there is no nearby BGPS source.

28.819+0.366: ND, position from ATCA-2014 data. Not observed at 6030-MHz as part of the Parkes MMB survey, nor was a 6030-MHz maser seen in the ATCA-2014 data. No radio/mm sources within $5''$, with the nearest ATLASGAL and BGPS sources 028.816+00.366 and G028.817+00.363 at angular offsets of 9.9 and $9.7''$ respectively.

30.778–0.801: ND, position from ATCA-2009. No radio/mm sources within $5''$ and no nearby ATLASGAL detection. The BGPS sources G030.772–00.801 and G030.782–00.795 are at angular offsets of $23.2''$ and $24.0''$ respectively. The nearest MMB CH_3OH maser G30.771–0.804 is at an angular separation of $29.0''$ making it very unlikely these are a true pair excited by the same source.

34.261–0.213: ND, position from ATCA-2009. No 1665-MHz detection from previous studies or 6030-MHz source in MMB MX data. No nearby radio or mm- continuum source reported within $5''$. At a separation of $25.1''$ the nearest MMB CH_3OH maser G34.267–0.210 is unlikely associated with this ex-OH source. The nearest mm/sub-mm sources are at similarly large separations and unlikely associated with the ex-OH maser, these sources being BGPS G034.264–00.210 (separation of $15.6''$) and AGAL 034.266–00.209 (separation of $23.5''$).

34.258+0.153: Known source. Here the 55kms^{-1} feature in left hand circularly polarised (LHCP) now dominates the source whereas in C03 the feature at 62.1kms^{-1} (LHCP) was dominant. Source detected at 6030-MHz. For this maser the nearest mm/sub-mm detections from BGPS and ATLASGAL are BGPS G034.258+00.154 and AGAL 034.258+00.154 with angular offsets between their reported

positions and the ex-OH maser peak of $1.4''$ and $2.5''$ respectively.

35.133–0.744: ND, position from ATCA-2013. No source seen in 6030-MHz MMB MX data. MMB CH_3OH maser G35.132–0.744 is located at a $2.0''$ separation from this ex-OH maser. Whilst there is no nearby BGPS source, ATLASGAL source AGAL 035.132–00.744 is at an angular separation of $3.3''$.

35.198–0.743: Known source at 1665-MHz (FC89) and 6035-MHz (C03) seen in absorption in the MMB 6030-MHz data. Over three epochs the 6035-MHz maser source has been increasing (by a factor 3.99 and 2.44 between its reported flux density in CV95 and C03 and the MMB result respectively, see Table 4). ATLASGAL detects a source (AGAL 035.197–00.742) offset from the maser peak position by $4.0''$. There is no nearby BGPS detection.

35.200–1.736: Known source at both 1665-MHz and 6035-MHz (FC89 and C03 respectively), see in absorption from MMB MX data at 6030-MHz. This maser source is seen to decrease in flux density between the two previous observations as reported by CV95 and C03 (by factors of -6.60 and -8.37 respectively). Interestingly in this time the polarization which displays peak emission at each epoch has switched handedness (Table 4). No ATLASGAL or BGPS detections within an arcminute.

40.282–0.220: ND, position and 6030-MHz detection from ATCA-2014. Not observed at 6030-MHz as part of the Parkes MMB survey. HCHII region at offset of $1.21''$ observed with the EVLA by [Sánchez-Monge et al. \(2011\)](#) and the MMB CH_3OH maser G40.425+0.700 is observed at an offset of $3.0''$. Sub-mm detection AGAL 040.283–00.219 has angular offset from the maser of $5.4''$, there is no BGPS source detected within an arcminute.

48.988–0.300: ND, position from ATCA-2009. Source BGPS G48.989–0.299 (mm source) offset by $4.47''$ and AGAL 048.991–00.299 (sub-mm) offset by $11.6''$. The MMB CH_3OH maser G48.990–0.299 by $8.9''$. No 6030-MHz detection.

49.046–0.290: ND, position from ATCA-2009. No 6030-MHz in MMB MX data and no detection at 1665-MHz in FC89, C98 or A00. No nearby radio or mm- continuum source reported within $5''$. This source is one of the ‘isolated’ ex-OH sources with no nearby CH_3OH detection discussed in §4.4.4, the nearest mm/sub-mm sources from the ATLASGAL and BGPS surveys are offset by $59.0''$ and $56.6''$ respectively, meaning there is likely no association between these detection and the ex-OH maser.

49.490–0.388: Known source, seen at 6035-MHz in C03 and 1665-MHz in FC89. Seen in absorption in the MMB 6030-MHz MX data. Nearby mm/sub-mm sources from ATLASGAL and BGPS are 049.489–00.389 (offset by $6.3''$) and G049.489–00.386 (offset by $7.7''$) respectively.

50.478+0.705: ND, ATCA-2009 position. Associated with IRAS 19194+1548 (IR 7.84 $''$). Source outside of range

of previous studies at 1665-MHz. No nearby radio or mm-continuum source reported within $5''$ and no ATLASGAL or BGPS detection within an arcminute. An ‘isolated’ ex-OH sources with the nearest CH_3OH maser over $595''$ away.

51.683+0.714: ND, ATCA-2014 position, this maser was not observed as part of the MMB MX at 6030-MHz and no maser was observed at 6030-MHz with our ATCA observations. Source outside of range of previous studies at 1665-MHz. No nearby radio or mm- continuum source reported within $5''$, no BGPS detection within an arcminute however the nearest ATLASGAL source AGAL 051.678+00.719 has an angular separation from the ex-OH maser peak of $22.5''$. The nearest MMB CH_3OH maser G51.679+0.719 is offset by $21.9''$.

284.016–0.856 ND, position from ATCA-2009. No 1665-MHz counterpart in C98 or FC89, no 6030-MHz counterpart in MMB MX spectra. There is no BGPS within an arcminute and the ATLASGAL source at the nearest angular separation is AGAL 284.016–00.857, $4.8''$ away. This source is an ‘isolated’ ex-OH source (discussed in §4.4.4) with no CH_3OH maser detected nearby by the MMB.

298.723–0.086 ND, ATCA-2009 position with maser covering very small velocity range, no 1665-MHz or 6030-MHz counterparts. Nearby is MMB CH_3OH maser G298.723–0.086 at an offset of $3.05''$. ATLASGAL source AGAL 298.724–00.086 is offset from the ex-OH maser peak by $3.6''$, no other nearby radio or mm- continuum source reported within $5''$.

305.208+0.206 ND, ATCA-2013 position, source previously detected at 1665-MHz (C98) where the source was significantly stronger (15.9Jy), than either hand of 6035-MHz detection (0.98(LHCP) and 1.25(RHCP) Jy). No 6030-MHz source in MMB MX data. SIMBA detection at 1.2-mm, G305.21+0.21, from [Hill et al. \(2005\)](#) with the 1.2mm peak offset by $4.42''$ from the maser peak position and an MMB CH_3OH maser, G305.208+0.206, separated by $0.57''$. AGAL 305.209+00.206 is offset by $2.0''$. There is no BGPS detected within an arcminute.

305.362+0.150 ND, ATCA-2009 position. Counterpart at 1665-MHz reported by C98, significantly brighter 10.6 (7.6)Jy than the 6035-MHz detection (0.41(LHCP) and 0.36(RHCP) Jy). No 6030-MHz seen in the MMB MX data. Candidate ultra-compact HII region, *G305.362+00.150*, in the G305 star-forming complex reported by [Hindson et al. \(2012\)](#) at a reported position offset from the ex-OH maser of $\sim 1.4''$. ATLASGAL detects source AGAL 305.362+00.151 at a similar separation of $2.0''$. There also exists the MMB CH_3OH maser G305.362+0.150 at an angular offset of $0.78''$.

308.056–0.396 Brightest newly detected source at 6035-MHz with a flux density of 15.93Jy (LHCP) and 25.46Jy (RHCP); interestingly no 6030-MHz counterpart seen in MMB MX data. No 1665-MHz detections C98. MMB CH_3OH maser G308.056–0.396 is offset for this ex-OH source by $1.2''$. Sub-mm source AGAL 308.057–00.397 is at an angular separation of $4.3''$.

308.651–0.507 ND, ATCA-2009 position, with no detected counterpart at 6030-MHz in MMB MX. There is no 1665-MHz detections in C98. MMB CH₃OH maser G308.651–0.507 is offset by 1.5'' and sub-mm core AGAL 308.652–00.507 at an offset of 2.1''.

309.384–0.135 ND at 6035-MHz from ATCA-2009. Weak detections at 1665-MHz (C98) of 0.23Jy. No 6030-MHz seen in MMB MX data. CH₃OH maser G309.384–0.135 from the MMB data is offset by 1.5'' and Extended Green Object (EGO) G309.38–0.13(a) present within 2.05'' (Cyganowski et al. 2008). At a similar angular offset (2.7'') is sub-mm AGAL 309.384–00.134.

309.901+0.231 ND, position from ATCA-2009. No 6030-MHz detection in MMB MX data and no 1665-MHz detection in C98. The MMB detected the nearby CH₃OH maser G309.901+0.231 which is offset from this ex-OH maser by 1.34'', this is a similar separation to AGAL 309.901+00.231 (offset 1.3''), the nearest sub-mm detection. The EGO G309.90+0.23 is within 4.4'' (Cyganowski et al. 2008).

312.598+0.045 ND, position from ATCA-2009. Known source at 1665-MHz (C98). No 6030-MHz detection in MMB MX data. Offset from sub-mm source G312.598+00.044 in the ATLASGAL survey by 4.46'' (Contreras et al. 2013).

320.427+0.103 ND with position from ATCA-2009. No 1665-MHz in FC98 or C98, no 6030-MHz detection in MMB MX data. Sub-mm source AGAL 320.427+00.102 is at an angular offset of 3.6''. The nearest MMB CH₃OH maser, G320.424+0.089, is at an angular offset of 50.5'' so is highly unlikely to be associated with the ex-OH detection.

326.447–0.749 and *326.448–0.749* Newly detected maser pair separated by 3.4'' with positions from ATCA-2009. Single 6030-MHz counterpart with similar velocity profile to *326.448–0.749*. Both sources within $\leq 3.5''$ of Young Stellar Object Candidate from the RMS survey (Mottram et al. 2007a). The pair are at angular separations of 6.5'' and 3.5'' from sub-mm source AGAL 326.449–00.749. The nearest MMB CH₃OH source to the pair is G326.448–0.748, offset by 5.5 and 2.5'' from *326.447–0.749* and *326.448–0.749* respectively.

327.944–0.115 ND, position from ATCA-2009. Beyond FC89 and A00 range and no detection of a 1665-MHz maser in C98. No 6030-MHz source in MMB MX data. The nearest MMB CH₃OH maser, G327.945–0.115, is at a separation of 3.7'' with no other nearby radio or mm-continuum source reported within 5'', the nearest sub-mm source in ATLASGAL (AGAL 327.948–00.117) is at an angular offset of 14.3'', meaning the maser and dense core are unlikely to be associated.

329.184–0.314 ND, position from ATCA-2009. No 6030-MHz MX data available for this source. 1665-MHz source from C98. CH₃OH maser G329.183–0.314 from the MMB is offset by 2.8''. Sub-mm source AGAL 329.184–00.314 is offset from the maser peak by 1.8''.

332.824–0.548: Known source. In both the 6035-MHz and 6030-MHz ATCA data there is a very strong continuum source (integrated flux density of 3.71 ± 0.03 Jy at 6035-MHz and 4.1 ± 0.3 Jy at 6030-MHz) at the same position as the 6035-MHz maser. There is no maser detected at 6030-MHz, instead this source appears in absorption. The nearest 6668-MHz CH₃OH maser is offset from the ex-OH detection by 7.0''. Figure 2 shows the continuum emission as contours along with the 6035-MHz maser position. This source is likely associated with the nearby HII candidate G332.8256–00.5498 seen in the RMS survey data (Mottram et al. 2007b), which is offset by 9.4'' and the sub-mm source AGAL 332.826–00.549 is at a separation of 4.2''.

332.964–0.679: ND with ATCA-2009 position. No 6030-MHz emission detected in the MMB MX. No 1665-MHz detection in C98. Separated by 2.1'' from EGO G332.96–0.68 (Cyganowski et al. 2008). The nearest MMB CH₃OH maser is G332.963–0.679 which is offset by 2.4''. The sub-mm source AGAL 332.962–00.679 is at an angular offset of 6.9''.

333.068–0.447: ND with ATCA-2009 position. No 6030-MHz or 1665-MHz detections from the MMB MX data and C98, respectively. G333.068–0.447 at an offset of 1.9'' is the closest MMB CH₃OH maser detected. The young stellar object (YSO) candidate G333.0682–00.4461(1) from the RMS survey is at an angular offset of 1.86'' (Mottram et al. 2007b). This YSO and the MMB CH₃OH maser G333.068–0.447 are co-spatial within the errors of the MMB ATCA data. The ATLASGAL source AGAL 333.068–00.447 is at a similar separation to the ex-OH maser of 1.9''.

333.228–0.055 ND, position from ATCA-2009. 1665-MHz detection in C98. No 6030-MHz source detected in MMB MX data. No nearby radio or mm-continuum source reported within 5'', with the nearest AGAL source over 30'' away. At an offset of 28.1'' the nearest MMB CH₃OH maser, G333.234–0.060, is unlikely to be associated with the same exciting source as the ex-OH maser.

337.097–0.929 ND, with position from ATCA-2013. This source was found in the Piggyback MX rather than the main survey MX as such there is no 6030-MHz MX data. No 6030-MHz maser was found in the ATCA-2013 data. No 1665-MHz source reported in C98. There is the sub-mm source AGAL 337.098–00.929 nearby at an angular offset of 2.4''. MMB CH₃OH maser G337.097–0.929 is at an offset of 5.3''.

337.844–0.374 ND, position from ATCA-2009. No 1665-MHz maser in FC89, C98 or A00. No 6030-MHz source in MMB MX data. Offset by $\sim 1.0''$ from IRAS 16367–4701 a source listed as an outflow candidate by Guzmán et al. (2012). At a similar offset, 1.24'', lies the MMB CH₃OH maser G337.844–0.375, at a greater offset but still potentially associated is the ATLASGAL source AGAL 337.844–00.376, which has a position offset from the ex-OH maser peak of 5.5''.

339.980–0.539 ND, from ATCA-2009. Non detection in 6030-MHz in MMB MX data. No 1665-MHz in C98 or FC89. Radio source GPSR 339.980-0.538 at 1.4GHz is offset by $1.77''$ (Zoonematkermani et al. 1990). At a larger offset of $2.6''$ is the MMB CH₃OH maser G339.980–0.538 and at greater still offset ($5.3''$) is compact sub-mm source AGAL 339.979-00.539.

341.974+0.225 ND, from ATCA-2009. Not detected in 6030-MHz in MMB MX data, nor is there a 1665-MHz maser in C98 or FC89. This maser is at an angular offset of $5''$ from sub-mm source AGAL 341.974+00.226. The nearest CH₃OH maser reported by the MMB is G341.973+0.233 at a separation of $29.8''$ so unlikely to exist around the same ionising source.

343.354–0.067 ND, ATCA-2009 position. No 1665-MHz detection in FC89, C98 or A00. No 6030-MHz emission seen in MMB MX. This source offset from the MMB CH₃OH maser G343.354–0.067 by $2.5''$. There are no other nearby radio or mm- continuum source reported within $5''$, with the nearest sub-mm source (AGAL G343.352–00.067) at an offset of $8.2''$.

344.419+0.044: In this known source the -72.5kms^{-1} feature (0.28Jy) from CV95 is missing in the MMB spectrum. No spectrum in C03 for comparison. The emission at $v=-65$ to -62.8kms^{-1} seen in the MMB MX spectrum is also seen in the CV95 spectrum but were then weak $\sim 0.1\text{Jy}$ compared to the now missing -72.5kms^{-1} feature.

345.495+1.469 ND, ATCA-2009 position. Two nearby 1665-MHz sources listed in C98, *G345.494+1.469* and *G345.498+1.467*. The 6035-MHz peak is closest to *G345.494+1.469* in velocity (peak velocity difference 0.4kms^{-1}). The ex-OH detection is positioned to the northeast of radio sources ‘C’ and ‘I-E’ detected toward IRAS 16562–3959 by (Guzmán et al. 2010). Object ‘C’ being the proposed central object and ‘I-E’ the inner eastern lobe of the collimated jet the authors detect toward this massive young stellar object. The nearest MMB CH₃OH maser, G345.498+1.467, to the ex-OH detection (offset by $13.12''$) is similarly positioned to the northeast of the ‘C’ and ‘I-E’ radio sources of Guzmán et al. (2010). In the same region is the sub-mm source AGAL 345.493+01.469 which is offset from the ex-OH maser by an angular separation of $6.3''$.

354.725+0.299 Detected in C03, however incorrectly listed with negative Galactic latitude.

357.924–0.338 ATCA-2009 position. No detection listed in C98 or A00 of 1665-MHz maser, no 6030-MHz detection in MMB MX. CH₃OH maser G357.924–0.337 from the MMB is offset by $3.9''$, beyond this no radio or mm- continuum sources are reported within $5''$ with the nearest sub-mm detection at a slightly larger separation of $5.5''$ (AGAL 357.923-00.337).

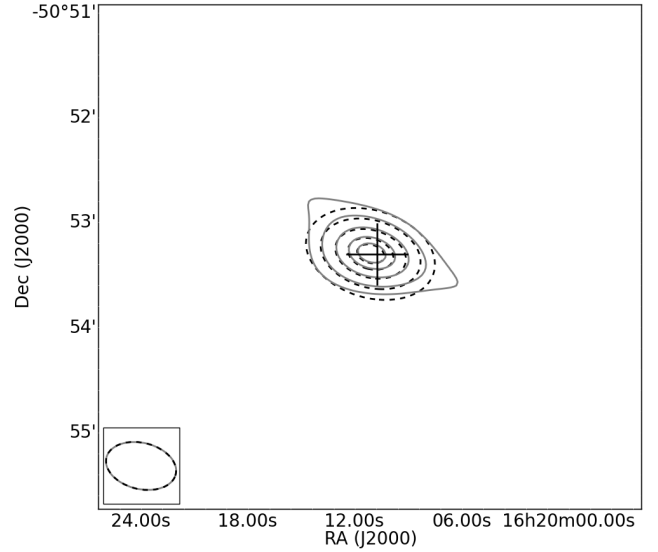


Figure 2. Continuum emission detected around source G332.824–0.548 at 6035-MHz (black dashed contour), and 6030-MHz (grey solid contour). Contours denote 10, 25, 50, 75 and 90% of the peak emission at each frequency (see text). The ‘+’ indicates the 6035-MHz ex-OH maser as observed in the ATCA-2013 data. The synthesised beam of each observation is given in the box at the lower left of the image.

3.2 Tentative or non-detections

Table 2 lists previously detected ex-OH sources for which the MMB survey MX shows no maser emission or a tentative detection that is below the MX observation noise. A tentative detection is considered such if there is structured emission at approximately the correct velocity of a previous detection (e.g. C03) but it falls below the 3σ RMS noise limit for the MX (listed in column 5 of Table 2). Non-detections show no such structure. Each of these sources is considered to have varied in flux density since its earlier detection to be below our detection threshold. The variability of masers in our sample is discussed in §4.5.

4 DISCUSSION

4.1 Galactic Distribution

The Galactic 6035-MHz maser population distribution as seen in our data can be seen graphically in Figure 3 (main panel). The leftmost and lower images in Figure 3 provide histograms of the distributions in Galactic latitude and longitude respectively.

4.1.1 Longitude Distribution

We have binned our ex-OH sample into 5 degree bins to look at the distribution of masers within the Galaxy, as seen in the lower image of Figure 3. Across the whole MMB survey longitude range there is an average maser count per 5° bin of 1.8, with a large standard deviation of 3.1. Including only bins with detections there are an average 4.7 masers per

Source MMBxOH-	RA [h m s]	Dec [d ' '']	V_{peak} [kms ⁻¹]	Upper limit [Jy]	Status N/T ^a
G003.910+0.001	17:54:38.74	-25:04:03.1	17.8	0.33	T
G022.435-0.169	18:32:43.83	-09:24:32.8	29.5	0.32	N
G040.623-0.138	19:06:01.64	+06:46:36.5	32.0	0.22	T
G285.263-0.050	10:31:29.88	-58:02:18.5	9.3	0.74	T
G306.322-0.334	13:21:23.02	-63:00:29.3	-23.5	0.21	T
G316.762-0.012	14:44:56.17	-59:48:00.7	-37.5	0.25	N
G319.398-0.012	15:30:17.41	-58:36:13.3	-12.7	0.25	N
G329.066-0.308	16:01:09.96	-53:16:02.3	-42.7	0.27	T
G336.358-0.137	16:33:29.19	-48:03:43.7	-75.1	0.38	N
G338.075+0.012	16:39:39.05	-46:41:28.3	-48.7	0.34	N
G338.280+0.542	16:38:09.07	-46:11:03.1	-56.8	0.33	N
G348.550-0.979	17:19:20.42	-39:03:51.6	-13.1	0.33	T

Table 2. List of previous ex-OH maser detections which were either non-detections or tentative (see text) in the MMB survey MX observations. Positions and velocities listed are from [Caswell \(2003\)](#). The upper limit listed in column 5 is $3\times$ the RMS noise in the MX for that source. ^a The status is either ‘N’ for non-detection or ‘T’ for tentative.

bin (with standard deviation of 3.4) implying a significant degree of clustering.

The majority of the survey range, between the survey boundary at 186° and 280° , is free from maser detections, with only two masers observed in this region (at $l=189.030^\circ$ and $l=240.316^\circ$) (1.6% of the total ex-OH sample). Given our smaller sample size this would not seem to contradict the detection rate in the CH₃OH survey which detected 22 CH₃OH masers (2.3% of the CH₃OH sample) in this same longitude range ([Green et al. 2012a](#)).

The clearest peak in the distribution is seen between 325° and 340° , the same longitude range as the Norma and Perseus (inner) tangent points ([Vallée 2014](#)). This peak in the distribution was also seen in the CH₃OH maser population of [Caswell et al. \(2011\)](#). This region contains 28.3% of the ex-OH masers detected by the MMB survey.

Another notable peak, when compared to those surrounding it, appears within the 305° and 310° bin. This coincides with direction of the Crux tangent point ($\sim 308^\circ$ [Vallée 2014](#)).

From 0° to the other survey boundary of 60° the distribution of masers is fairly uniform, with only a notable dip between 20° and 25° and a tail-off after 50° . The former is likely due to observations being made through the inter-arm region of the Perseus and Sagittarius arms toward the distant Perseus arm.

4.1.2 Latitude Distribution

Of the 127 ex-OH masers 94% are within 1° of the Galactic plane. Of those outside this latitude range 2 are new detections. In the MMB main survey catalogues ([Caswell et al. 2010, 2011](#); [Green et al. 2010, 2012a](#); [Breen et al. 2015](#)) (hereafter the MMB catalogue papers), of the 972 6668-MHz masers 911 (94%) were found to be within 1° of the Galactic plane, the same percentage seen in the 6035-MHz sources, indicative that the population of sources being traced by both species is comparable. The region with most 6668-MHz masers at latitudes more extreme than $|b| \geq 1^\circ$ was in the longitude range 186° to 330° ([Green et al. 2012a](#)) with 15% of detections at high/low latitudes. Our small number of 6035-MHz masers (30) in this region does not allow for a

robust comparison however 7% of detections are found at $|b| \geq 1^\circ$, which is more consistent with the general trend of 6035-MHz and 6668-MHz within the whole Galaxy.

4.2 Velocity distribution and Galactic structure.

Figure 4 shows the longitude-velocity ($l-v$) positions of the observed ex-OH masers overlaid on the spiral arm structure of the Milky Way. The spiral arm positions follow the logarithmic spirals of [Georgelin & Georgelin \(1976\)](#) with the [Taylor & Cordes \(1993\)](#) adjustments. We use the [Reid et al. \(2009\)](#) rotation curve to calculate the V_{lsr} of the spiral arms. The 3-kpc arms in Figure 4 (grey regions) are as per [Dame & Thaddeus \(2008\)](#). We use these models in order for the plot to be directly comparable with the latest of the MMB catalogue papers. We discuss the velocity range and number count of ex-OH masers in comparison to CH₃OH using the same longitude ranges as the MMB catalogue papers.

4.2.1 Longitude $345^\circ - 006^\circ$, MMB Paper I

In the region covering the Galactic Centre we find 23 ex-OH masers, 18.1% of the total, covering a velocity range of -97 to 92 kms⁻¹. There is a significant overlap of all the Galactic spiral arms within this longitude range making comment on maser association with specific spiral arms difficult, however those masers near the extrema of our velocity range do have $l-v$ properties which indicate they are within the near (high negative v) or far (high positive v) 3-kpc arms. These comprise four sources; $347.628+0.149$ and $351.581-0.353$, at negative velocity thus in the near 3-kpc arm plus $0.666-0.029$ and $0.666-0.035$ at low l but high v making them candidates for inhabiting the far 3-kpc arm. However [Caswell et al. \(2010\)](#) point out that for the latter pair star formation tracing masers in this region are more likely to be part of the Sgr B2 star forming complex. The most extreme positive velocity source in this l range is $354.725+0.299$ at a velocity of $+91.76$ kms⁻¹, which, as can be seen in Figure 4, makes it an outlier with respect to the spiral arm structure of the Milky Way.

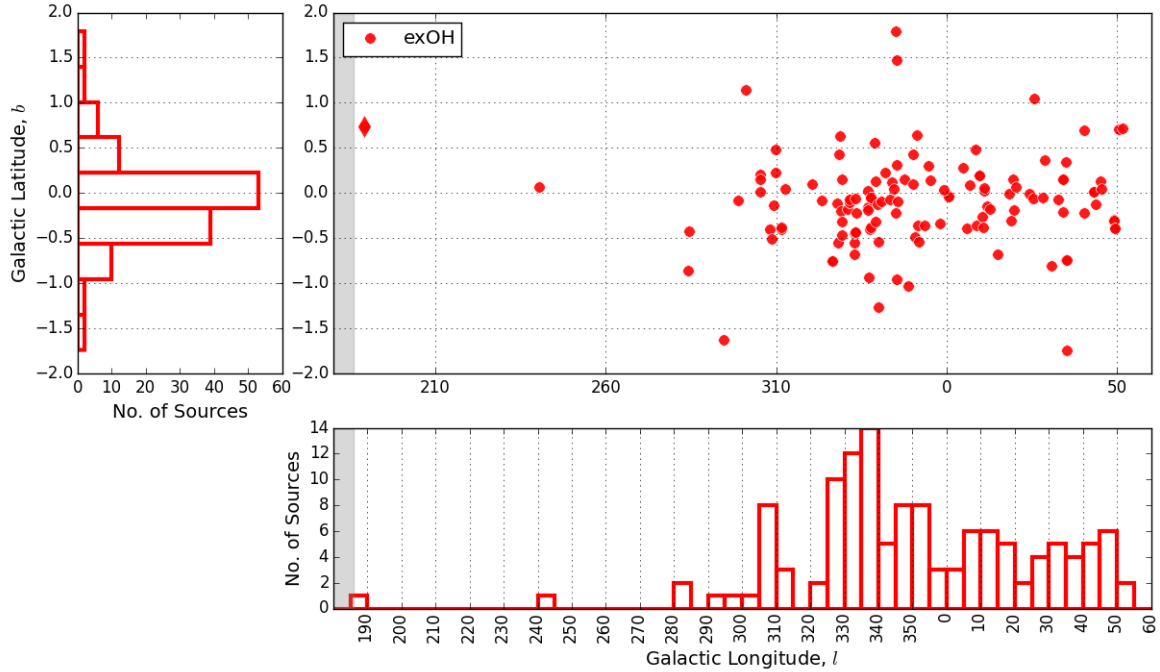


Figure 3. Galactic distribution of detected ex-OH masers within the MMB survey region. *Top right:* Positions of ex-OH detected during the MMB survey, the grey region between 180° and 186° is not covered by the survey. The source $189.030+0.783$, is marked as a diamond to highlight that this source’s position comes from the Parkes data only. *Top left:* Histogram of ex-OH distribution in Galactic latitude, b . *Bottom:* Histogram of ex-OH distribution in Galactic longitude, l , grey region as per *top right* plot.

Caswell et al. (2010) found 183 CH₃OH masers in this region, 18.9% of the CH₃OH total, comparable to the proportion of ex-OH in our sample. The velocity range covered by these masers is -127 to 104 km s^{-1} exceeding the ex-OH velocity range of -97 to 92 km s^{-1} seen in our sample. Two methanol masers G354.701+0.299 and G354.724+0.300 from this region display peculiarly high positive velocities for the longitude, which are ascribed to these sources being in the Galactic bar. Our unusual ex-OH source $354.725+0.299$ is separated spatially by $3.66''$ and 2.14 km s^{-1} from G354.724+0.300 placing it also in the Galactic bar.

4.2.1.1 The Central Molecular Zone: In recent years (since the publication of Caswell et al. 2010) there has been significant advancement in the understanding of the orbital behaviour of molecular gas in the central molecular zone (CMZ) of the Milky Way.

The orbital properties of molecular gas in the inner 250pc ($l \approx \pm 1.7^\circ$) of the Milky Way have been found to display an eccentric (about Sgr A*), open (rather than closed) and warped (having vertical motion) orbit (Longmore et al. 2013; Kruijssen et al. 2015; Henshaw et al. 2016).

In this region we find four ex-OH masers $0.666-0.029$ and $0.666-0.035$ which Caswell et al. (2010) previously associated with Sgr B2 and $357.924-0.338$ and $359.137+0.031$. Using the best-fit orbital solution of Kruijssen et al. (2015) (plotted as black dot-dash in Figure 4) we find that indeed $0.666-0.029$ and $0.666-0.035$ seem

to indeed fall very well on this orbital path toward the position of Sgr B2. $357.924-0.338$ is at too low a latitude to be expected to follow the CMZ orbit and $359.137+0.031$ lies outside of this orbital path and at velocities more consistent with association with one of the spiral arms.

4.2.2 Longitude $006^\circ - 020^\circ$, MMB Paper II

Within this longitude range we detect 16 ex-OH sources, 12.6% of total, which display a velocity range of -2.3 to 117.8 km s^{-1} . In $l - v$ space there is a significant portion of all the major Galactic spiral arms within this l range, though it does appear that most of our negative velocity ex-OH masers are likely within the Norma arm rather than the Crux-Scutum arm (see Figure 4).

Green et al. (2010) catalogued 119 CH₃OH masers in this longitude range, 12.24% of the CH₃OH total. Again the ex-OH and CH₃OH proportion with respect to the source totals are comparable. The velocity range, -30.2 to 157 km s^{-1} , of the CH₃OH masers exceeds that of the ex-OH sample, particularly for those few sources with negative velocity $< -10 \text{ km s}^{-1}$ which are thought to be part of the near 3-kpc arm. Also unlike the CH₃OH survey we do not appear to have detected any ex-OH masers in the far 3-kpc arm, which contains the CH₃OH sample’s high positive velocity sources in this region.

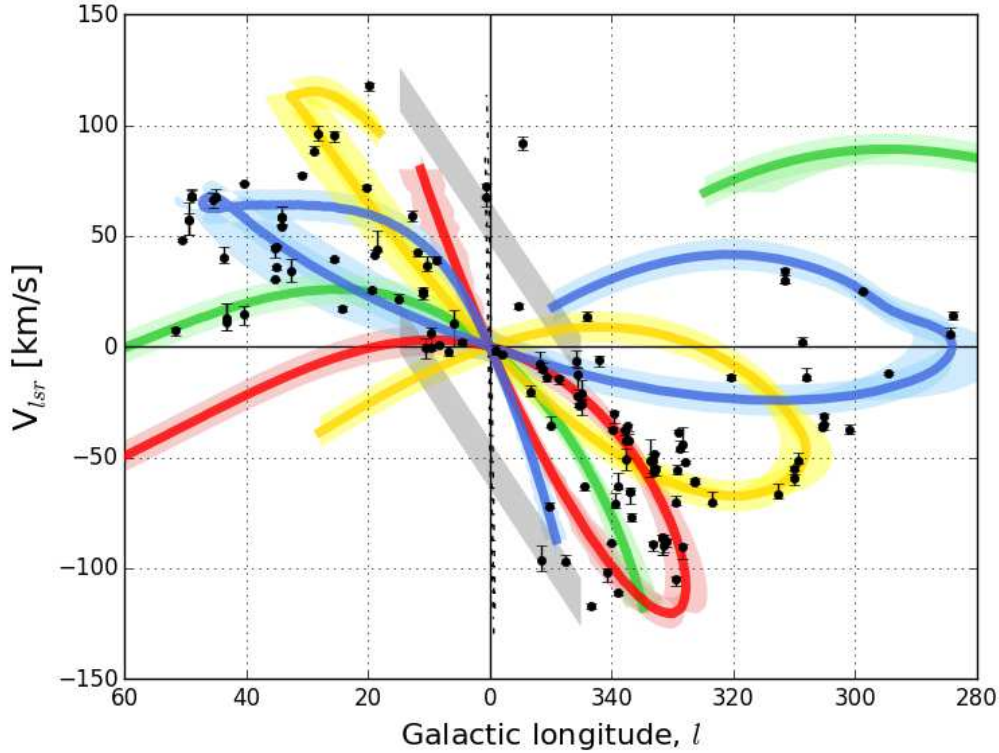


Figure 4. l - V_{lsr} distribution of ex-OH masers within the galaxy. ex-OH sources are plotted as black circles at the source peak velocity, the errorbars give the velocity range of the maser source. The spiral arms (coloured as Norma -red, Carina-Sagittarius - blue, Perseus - green, Crux-Scutum - yellow, Local arm - broken pink) follow Georgelin & Georgelin (1976) modified by Taylor & Cordes (1993), using the Reid et al. (2009) rotation curve. The dark central bands in each colour show the loci of each arm with the paler shaded regions showing the parameter space covered by arms of width 1kpc with velocity $\pm 7\text{km s}^{-1}$ that of the loci. The near and far 3kpc arms are represented as grey regions, following Dame & Thaddeus (2008). The thin black dot-dash line around $l = 0^\circ$ shows the best-fit open orbit model for molecular clouds in the CMZ from Kruijssen et al. (2015). Note: For clarity of the majority of sources the x -axis has been truncated and that two sources exist at $l < 280^\circ$.

4.2.3 Longitude 330° - 345° , MMB Paper III

A total of 30 ex-OH masers are found within this longitude range, 23.6% of total, covering a velocity range of -116.9 to 13.7 km s^{-1} . Figure 4 shows this region contains a significant part of the Norma, Crux-Scutum and Perseus Arms, with the majority of our sources appearing in the region of $l-v$ space where Norma and Crux-Scutum overlap.

The 198 CH_3OH masers found within this region make up 20.4% of total CH_3OH population. This value differs by $\sim 3.2\%$ from the ex-OH result, with a greater fraction of ex-OH found within this longitude range, though given the smaller ex-OH population this value is within counting statistics and may not be significant.

The CH_3OH maser velocity range covers -127 to 19 km s^{-1} with just two sources contributing positive velocities. The ex-OH sample contains only a single source with positive velocity 343.929 ± 0.125 which is positionally coincident with CH_3OH maser G343.929+0.125, one of the two contributing the positive velocity from the CH_3OH survey.

4.2.4 Longitude 186° - 330° , MMB Paper IV

We find 30 ex-OH masers within this area of sky (23.6% of the total). ex-OH masers in this region exhibit velocities in the range of -104.7 to 63.6 km s^{-1} . This region contains a large section of the Crux-Scutum and the Carina-Sagittarius arms as well as a section of the Perseus arm (unconfused at high velocity $> 63\text{ km s}^{-1}$) and the Norma tangent. We find two ex-OH masers within the Perseus arm which exists in this region, 189.030 ± 0.738 and 240.316 ± 0.071 (not seen in Figure 4 due to the truncated x -axis). The remainder of our masers in this region trace the remaining spiral arms well.

Green et al. (2012a) report 207 CH_3OH masers comprising 21.3% of the total MMB CH_3OH sample a comparable percentage to our ex-OH statistics.

4.2.5 Longitude 020° - 060° , MMB Paper V

In this region we find 28 ex-OH masers inhabit this l range, (22.1% of total) over a velocity range 7.1 to 96.1 km s^{-1} . Notably in Figure 4, no ex-OH masers in our sample appear associated with the negative velocity components of the Norma or Crux-Scutum arms present in this l range.

Breen et al. (2015) catalogued 265 CH₃OH masers in this region, 27.3% of the total. The proportion of CH₃OH masers detected with respect to the total source counts is 5.2% greater than ex-OH masers, suggesting an underabundance of the latter species in this region.

The velocity range of CH₃OH sources is -42.8 to 125.5 km s⁻¹ appearing far greater than that of ex-OH, though in fact the majority (79%) of CH₃OH masers fall within the same range of ex-OH with only 12 masers having $V < 0$ km s⁻¹ and 43 appearing above 100 km s⁻¹.

4.3 6030-MHz ex-OH masers associated with 6035-MHz masers

We detect 32 6030-MHz ex-OH masers within the same sources as 6035-MHz masers in our catalogue, however there are 11 6035-MHz masers from our catalogue for which there is no 6030-MHz MX data and one for which there exist only RHCP data. Disregarding these 12 sources, 28% of our 6035-MHz sample has a 6030-MHz counterpart. Previous studies of these two ex-OH transitions found percentages of 36% (Caswell 2003). We account for the difference between these two values in three ways. Firstly, by the fact that the MMB data have a typical MX RMS ~ 0.1 Jy (Green et al. 2009) which is higher than the typical spectrum RMS (0.03-0.05 Jy) reported by Caswell (2003) for their data. This may allow for the detection by Caswell (2003) of more lower flux density 6030-MHz counterparts than we were capable of, thus boosting their percentage. Secondly, the MMB is a complete untargeted survey meaning we may be seeing a number of sources at different evolutionary stages to that of the sample in Caswell (2003), which collated targeted surveys toward strong OH emission sites (Caswell 1997) and ground-state OH masers (Caswell 1998, 2001). Finally, given the variability of the ex-OH transition (see section 4.5 for a discussion of this in the 6035-MHz line) a number of weak 6030-MHz masers previously detected maybe too weak for detection in our survey.

4.3.1 Flux density comparison

Figure 5 compares the peak flux density of the 6035-MHz maser emission with that of the counterpart source at 6030-MHz at its peak velocity. The largest velocity offset between the two maser species peak emission seen in our data is 5.0 km s⁻¹ in source 49.490-0.388 (a feature also seen by C03), as such this is not included in Figure 5.

For the remainder of sources the velocity displacement between peaks at the different frequencies is always below 2.6 km s⁻¹. Where there is a 6030-MHz ex-OH maser associated with a 6035-MHz maser, the 6030-MHz peak flux density never exceeds the counterpart 6035-MHz maser value. This result is consistent with the ex-OH maser model results of Gray et al. (1992), Cragg et al. (2002) and the majority of observational results (e.g. Baudry et al. 1997; Desmurs & Baudry 1998; Caswell 2003). Baudry et al. (1997) report 6030/6035-MHz typical flux density ratios of 0.14 to 0.5, and similarly Caswell (2003) reports a typical values of 0.125, up to extremes such as 0.01. Such values are consistent with our findings (Figure 5).

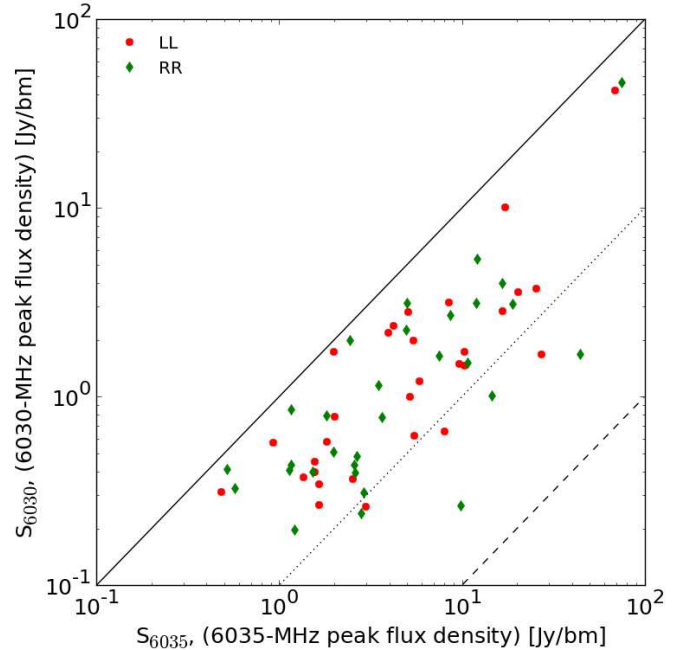


Figure 5. Peak 6035-MHz ex-OH flux density, S_{6035} , compared to peak 6030-MHz ex-OH flux density, S_{6030} . Solid line $S_{6035} = S_{6030}$, dotted line $S_{6030} = 0.1 \times S_{6035}$, dashed line $S_{6030} = 0.01 \times S_{6035}$.

4.4 Methanol maser association

The works of Ellingsen et al. (2007) and Breen et al. (2010a) suggest that masers of different species provide an evolutionary time line of regions of high-mass star formation. The simultaneous occurrence of class II CH₃OH and ground-state OH masers occurs later on in the relative lifetime of a high-mass star formation region (Breen et al. 2010a, see their Figure 6.), whilst it remains unclear about the association epoch of class II CH₃OH and ex-OH species. Given our sample of ex-OH masers are drawn from the same Galactic plane survey as the class II CH₃OH masers we are in a position to give robust information on the association rates of the two species.

4.4.1 Angular Separation

For each of the observed ex-OH masers the closest class II CH₃OH maser (in terms of angular separation) was determined; the CH₃OH maser positions were taken from the MMB catalogues. Figure 6 shows the distribution of angular separation between our ex-OH masers and the nearest class II CH₃OH masers. Within this figure we show only sources with angular separations, $\theta \leq 30''$ (equivalent to ~ 1 pc at a distance of 5 kpc). Sources at larger separations, referred to hereafter as ‘isolated’ ex-OH masers, are discussed in §4.4.4.

As can be seen in Figure 6 the majority of ex-OH masers, $\sim 80\%$, are within $\theta \leq 10''$ (~ 0.25 pc at 5 kpc) of a CH₃OH maser, where one would assume that the majority of these sources are associated with the same star forming core (nominal size ~ 0.1 pc), forming one or more stellar sources.

Of this 80% the largest proportion (64 sources), are within $2''$ (~ 0.05 pc at 5 kpc) a separation at which one may assume both are associated with the same protostellar object (c.f. the fiducial size of a hyper compact HII region ($\lesssim 0.03$ pc), e.g. Kurtz 2005).

In their pilot study of ground-state OH masers in Carina-Sagittarius Green et al. (2012b) use an association limit of ‘coincident within the positional errors’. Applying this same limit to our ex-OH data ($0.4''$, 9.7 mpc at 5 kpc) we find 26 sources meeting this criteria, for these sources one would confidently assume each maser species are part of the same protostellar system.

Figure 7 plots the peak velocity of each maser species against its nearest counterpart for all sources with an ATCA position and clearly shows that there is a tight correlation between the two masing species across all velocities. Figure 8 gives the velocity difference, ΔV , of potential ex-OH - CH₃OH maser pairs plotted against the angular separation of the sources. In this figure it can be seen that the majority of ex-OH masers are within ± 5.0 km s⁻¹ (denoted by the two green horizontal dashed lines) of their positional counterpart CH₃OH maser. This is particularly true for those sources with angular separations of $\theta \leq 2''$ (left of the vertical dotted line), with only 5 of 64 sources outside the ± 5.0 km s⁻¹ range, and $2'' < \theta \leq 10''$ (left of the vertical dot-dash line), with 7 of 37 sources outside this range.

Also indicative of true associations for the majority of low angular separation maser pairs is the fact that the mean $|\Delta V|$ increasingly deviates from $|\Delta V| = 0$ from the $\leq 2''$ grouping through $2'' < \theta \leq 10''$ up to the $\theta > 10''$ group (see column 3 in the upper portion of Table 3). There is also an increase in the standard deviation (column 4 Table 3) between the each group.

4.4.2 Physical Separation

A large number of MMB methanol sources were assigned a distance in Green & McClure-Griffiths (2011), which used HI self-absorption data to resolve the near/far kinematic distance ambiguity for these masers. Of our sample of 126¹ ex-OH masers 118 have likely associated CH₃OH counterparts in the Green & McClure-Griffiths (2011) study.

Additionally, Reid et al. (2014) have released parallax distance measurements of a large number of CH₃OH (both 6.7 and 12.2 GHz) masers, eight of which are likely counterparts to our ex-OH and the MMB sources. For these sources we use the parallax distance in place of the HI self-absorption distance. Sources for which the near/far distance ambiguity remains, i.e. they have no HI or parallax distance, are not considered further in this association analysis, nor are sources where the ex-OH and CH₃OH maser are separated by $\geq 30''$. Leaving 91 potential maser pairs.

Assuming that these 91 ex-OH and CH₃OH potential pairs both exist at the same distance we can repeat the analysis from the previous section using physical, Θ , rather than angular separation.

The lower panel of Table 3 presents this quantitatively. We divide our sample into maser pairs of separations \leq

0.03 pc (the HCHII size scale), between $0.03 \text{ pc} < \Theta \leq 0.1 \text{ pc}$ (between HCHII and protostellar core size scale) and greater than 0.1 pc. Again we find an increase in mean $|\Delta V|$ with increasing separation, indicative of looser association between species. Figure 9 follows Figure 8, but using the physical separation between maser species for those with assigned distances from Green & McClure-Griffiths (2011) or Reid et al. (2014). We find that only four sources of forty-one in our smallest physical separation group have $|\Delta V| > 5 \text{ km s}^{-1}$ (left of dotted line).

From this, one could take a *very* conservative lower limit of true associations with the 972 class II CH₃OH masers from the MMB as being 37 ex-OH sources; at separations ≤ 0.03 pc with $|\Delta V| \leq 5 \text{ km s}^{-1}$.

4.4.3 Ex-OH maser lifetimes

van der Walt (2005) used a statistical analysis of the then known number of 6668-MHz CH₃OH masers in the Milky Way to estimate the lifetime of an individual CH₃OH maser source, finding a value of between 2.5 and 4.5×10^4 years. Taking this value and the occurrence of associated pairs between the MMB CH₃OH and ex-OH masers (29.4%) we can calculate a lifetime for an ex-OH maser source.

Firstly, we assume that ex-OH and 6668-MHz CH₃OH masers are associated for a single period during the formation of a high-mass star and that all our associated pairs are forming in high-mass star forming regions². Given these assumptions the timescale for coexistence for these maser species can be calculated:

$$\tau_{\text{coexist}} = \frac{N_{\text{meth+exOH}}}{N_{\text{meth}}} \tau_{\text{meth}} \quad (1)$$

where τ_{coexist} is the time of species coexistence, $N_{\text{meth+exOH}}$ the number of associated ex-OH and CH₃OH pairs in our survey, N_{meth} the total number of CH₃OH maser in the same survey region and τ_{meth} the CH₃OH maser lifetime as calculated by van der Walt (2005). Using our conservative lower limit of 37 maser pairs and the total of 972 CH₃OH maser in the MMB catalogues this gives a timescale of coexistence for these maser species of 950 to 1700 years.

This coexistence timescale allows us to next estimate the lifetime of the ex-OH masers themselves. We find 29.4% of our sample are coexisting with CH₃OH masers, which is equivalent to the ex-OH masers spending 29.4% of their total lifetime in associated with CH₃OH meaning that the total lifetime, τ_{exOH} , can be calculated using the equivalent formula to 1:

$$\tau_{\text{coexist}} = \frac{N_{\text{meth+exOH}}}{N_{\text{exOH}}} \tau_{\text{exOH}} \quad (2)$$

where N_{exOH} is the total number of ex-OH maser in our sample and other symbols have their previous meanings. Following this approach we calculate that the total lifetimes of ex-OH maser sources are between 3.3×10^3 to 5.8×10^3 years. If we expand our associated sample ($N_{\text{meth+exOH}}$) to include all sources with separations less than 0.1 pc with $|\Delta V|$

¹ We exclude 189.030+0.738 for this analysis due to its low accuracy position (see § 3)

² 6668-MHz CH₃OH maser have never been detected outside of high-mass star forming regions (Minier et al. 2003; Xu et al. 2008; Breen et al. 2013).

between $\pm 5.0 \text{ km s}^{-1}$ this gives 55 associated pairs, a coexistence timescale of 1400 to 2500 years and an estimated lifetime of 4.6×10^3 to 8.3×10^3 years for ex-OH. This value is shorter than that expected of the ground-state OH maser of a *few* $\times 10^4$ years (Fish & Reid 2006).

Finally, we note two caveats relevant to the above calculated values. First we do not take into account the potential existence of ex-OH masers around post main sequence stars, but given the rarity of such masers and the lack of detection of such sources in our sample (see §4.4.4) the effect of such contamination on the estimated value will be of the order of a few percent, much smaller than the estimated lifetime ranges we calculate. Second, if the assumption that 6668-MHz CH₃OH masers and ex-OH masers exist at only a single epoch during star formation is not true then our values would act as an upper limit for ex-OH maser lifetime.

4.4.4 Isolated ex-OH sources: Separation $\geq 30''$

From Figure 8 it can also be seen that 11 ex-OH sources have separations from the nearest CH₃OH maser greater than $100''$ up to $764''$ which at a fiducial 5kpc distance to a high-mass star forming region gives a separation in excess of 2pc up to 18.5pc. Whilst this separation is sufficiently small that the sources could reside in the same giant molecular cloud (typical size 100pc see e.g. Larson 2003), which may account for some of the low ΔV values for these sources, it is very unlikely that these masers are truly associated and being excited by the same source. Beyond this, there are a further three sources which appear truly isolated with no counterpart from the MMB catalogues found within tens of arcminutes, these being $8.352+0.478$, $240.316+0.071$ and $284.016-0.856$.

We inspected the literature for counterparts to these three extremely isolated masers, finding an interesting diversity of star formation tracing counterparts between them. Source $8.352+0.478$ has no counterpart dense core in either BGPS or ATLASGAL within $30''$ and no other maser species detections within $1.0''$. Source $284.016-0.856$ similarly has no other maser species present within $1.0''$, but does (as noted in § 3.1) have a likely associated dense core AGAL $284.016-00.857$ offset by $4.8''$. The source $240.316+0.071$ has a close, $1.0''$, water maser counterpart listed in both Breen et al. (2010b) and Reid et al. (2014) and a ground-state OH maser at an offset position of $0.74''$. This source is outside of the survey range for both BGPS or ATLASGAL, but does have nearby, $1.0''$ millimetre and radio wavelength detections associated with the (ultra) compact HII region G240.31+0.07 (see e.g. Chen et al. 2007; Trinidad 2011). Finally, the literature provides no nearby ($\leq 30''$) evolved/post main sequence star counterparts for any isolated maser sources suggesting that these masers are associated with star formation.

In the modelling of Cragg et al. (2002) it was found that the 6035-MHz ex-OH maser can exist at densities up to $n_H = 10^{8.5} \text{ cm}^{-3}$ which exceeds the density at which the 6668-MHz CH₃OH maser is quenched by collisional interaction ($n_H = 10^{8.3} \text{ cm}^{-3}$). The isolated ex-OH masers we detect may be tracing these extreme high density regions and warrant further investigation to examine their environments.

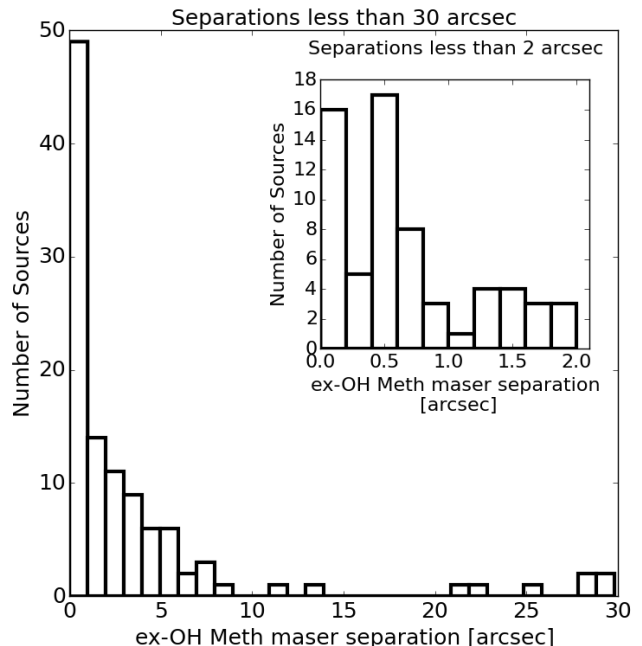


Figure 6. Histogram of ex-OH to nearest class II CH₃OH maser from the MMB survey for separations $\leq 40''$. The inset figure shows the distribution of separations $\leq 2''$ equivalent to ~ 0.05 pc at 5kpc.

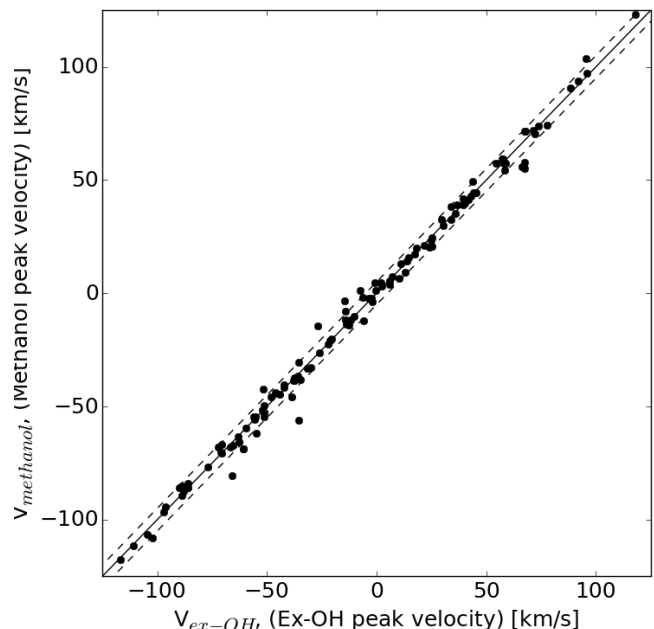


Figure 7. Peak V_{methanol} plotted against peak $V_{\text{ex-OH}}$ for nearest maser pairings for sources separated by less than the ATCA primary beam at 6035-MHz ($569''$). The solid line gives $V_{\text{methanol}} = V_{\text{ex-OH}}$ and the dashed lines $V_{\text{methanol}} = V_{\text{ex-OH}} \pm 5.0 \text{ km s}^{-1}$.

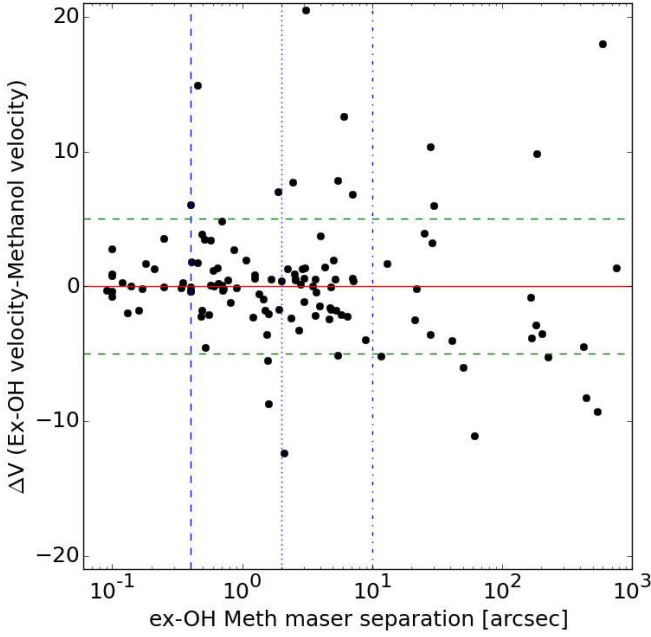


Figure 8. The velocity difference between ex-OH masers and the nearest CH₃OH maser as a function of angular separation of the pair. The horizontal red (solid) and green (dashed) lines denoted ΔV of 0km s^{-1} and $\pm 5\text{km s}^{-1}$ respectively. The vertical dotted and dash-dot line mark out angular separations of 2 and $10''$ respectively. *Note: the log x-axis excludes those few sources where the maser coordinates are identical thus having a separation of zero.*

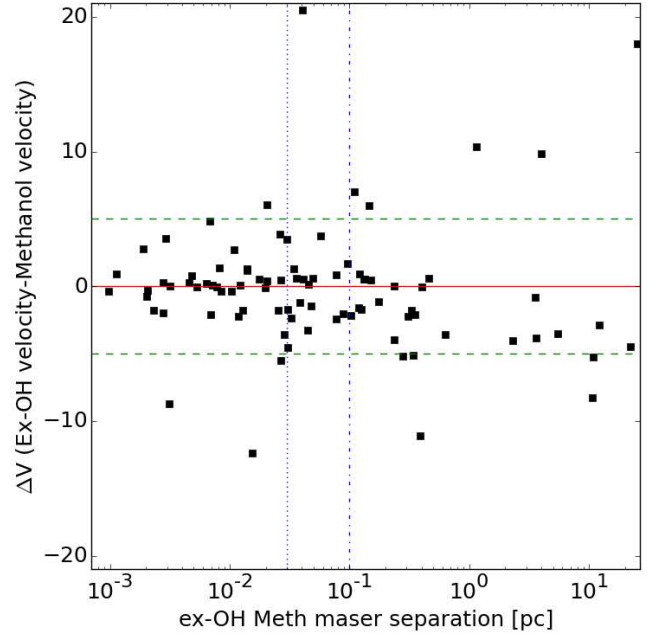


Figure 9. The velocity difference between ex-OH masers and the nearest CH₃OH maser as a function of physical separation of the pair, for sources with distances from [Green & McClure-Griffiths \(2011\)](#) only. The horizontal red (solid) and green (dashed) lines denoted ΔV of 0km s^{-1} and $\pm 5\text{km s}^{-1}$ respectively. The vertical dotted and dash-dot line mark out angular separations of 0.03 and 0.1 pc respectively. *Note: the log x-axis excludes those few sources where the maser coordinates are identical thus having a separation of zero.*

ex-OH - CH ₃ OH Separation	No. of sources	$ \Delta V _{\text{mean}}$ [km s ⁻¹]	ΔV_{std} [km s ⁻¹]
$\leq 0.4''$	26	1.06	1.64
$\leq 2''$	64	1.85	3.04
$2'' < \theta \leq 10''$	37	3.12	5.19
$> 10''$	23	5.46	6.74
$\leq 0.03\text{pc}$	41	1.93	3.15
$0.03\text{pc} < \theta \leq 0.1\text{pc}$	18	2.23	3.72
$> 0.1\text{pc}$	32	4.04	5.59

Table 3. ex-OH - CH₃OH maser separation distribution. *Upper panel*, angular separation (in arcseconds) for all sources. *Lower panel* physical separation (in parsec) for sources with [Green & McClure-Griffiths \(2011\)](#) or [Reid et al. \(2014\)](#) distances only. Column 3 gives the mean velocity difference between positionally associated ex-OH - CH₃OH pairs from the Stokes I peak, and Column 4 the standard deviation of these values.

4.5 Variability

To inspect the variability of the ex-OH sources over time a comparison of the flux densities for sources observed in either CV95 and/or C03 and the MMB MX's was made. The MMB MX data was obtained 2008/2009, CV95 data were mostly taken in 1993/1994, giving a minimum time baseline of 14 years. The C03 data were taken in 2001 giving a minimum time baseline of 7 years. The CV95/C03

reported peak flux densities and spectra were inspected to ensure that for sources which we had an MX, the CV95/C03 peak was within 1.0km/s of the MX peak for the same polarisation. Only masers where the peak matched in velocity and polarisation were used in the comparison, thus excluding those with multi-component spectra where a different velocity component now dominates (as discussed in §3.1).

In total the comparison was made with 61 sources from CV95 and 77 sources from C03. Figure 10 plots the comparison of the MMB peak flux densities, including the sources which were found to be tentative or non-detections from the MMB MX data (see §3.2) for which 3σ upper limits were used. The ratios of flux densities for CV95/MMB and C03/MMB have median values of 0.92 and 0.94 respectively, but as can be seen from Figure 10 a number of sources, 19 from CV95 and 11 from C03, have varied by a factor of ≥ 2 over at least one of the two periods. These highly variable sources are listed in Table 4. For those sources where the variation is ≥ 2 over only one epoch, the variation over the other epoch is also listed (where possible) to highlight any trend within the variation.

The majority of these highly variable sources show the variation acting in the same direction, either increasing or decreasing, over both epochs to the MMB. Four sources ($19.486+0.151$, $49.486-0.389$, $345.003-0.224$ and $345.487+0.314$) have variation acting in the opposite direc-

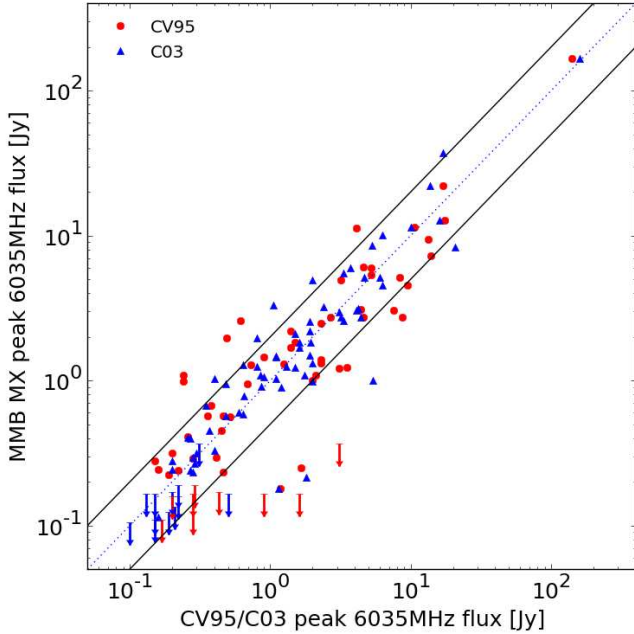


Figure 10. Comparison of ex-OH masers observed as part of the MMB with those previously observed in CV95 (red) and C03 (blue), sources which are tentative or non-detections (see §3.2) are marked as downward arrows of the same colour. The dashed line indicated $y=x$, and the solid lines $y=2x$ and $y=x/2$.

tion between the CV95-MMB and C03-MMB epochs. An additional 4 sources ($11.904-0.141$, $15.035-0.677$, $35.200-1.736$ and $345.010+1.792$) show a switch in sense of variation between the CV95 to C03 and the C03 to MMB measurements, but had sufficient variation over the CV95 to MMB period to show an overall continuing positive or negative trend when comparing CV95-MMB and C03-MMB. For these 8 sources the variation must have reached a maximum/minimum at some point between either CV95 and C03 or C03 and MMB observations which may be indicative of variation on a timescale of years or less in these sources, making them interesting candidates for single dish monitoring observations.

5 SUMMARY

We present the results from the first complete Galactic Plane survey of ex-OH masers at 6035-MHz. This survey was carried out as part of the Methanol MultiBeam Survey using the Parkes 64-m radio telescope. The catalogue of sources comprises 127 sources with 47 new detections. All the new detections have high accuracy positions from interferometric observations with the ATCA. In addition to the measured 6035-MHz sources we also catalogue associated 6030-MHz ex-OH masers, detecting 32 masers at this frequency. The 6030-MHz emission is typically weaker than at 6035 consistent with previous studies.

The catalogue is compared to the main MMB catalogue of 6668-MHz CH_3OH masers (comprising 972 detections),

from which we find an unambiguous association (sources separated by $\leq 0.4''$, $\leq 9.7\text{mpc}$ at 5kpc) for just 26 sources. Increasing the association limit to $2''$ (0.05pc at 5kpc, the approximate scale of a single proto-stellar core) we find 64 CH_3OH –ex-OH pairs. In our sample 91 ex-OH sources have a robust distance measurements allowing physical separations to be calculated. Of these we find 37 likely CH_3OH –ex-OH maser pairs with physical separations of $\leq 0.03\text{pc}$ and 55 pairings separated by $\leq 0.1\text{pc}$.

Assuming a single epoch of coexistence of CH_3OH and ex-OH masers around a high-mass protostellar source and using the [van der Walt \(2005\)](#) estimated CH_3OH maser lifetime, we are able to put constraints on the coexistence period of the two maser species and the ex-OH maser lifetime, using our associated pairs with distance measurements. We find a period of maser overlap of $0.95 - 2.5 \times 10^3$ and a lifetime for ex-OH masers of $3.3 - 8.3 \times 10^3$ years.

Finally we compare the observed peak 6035-MHz emission to that observed at previous epochs by [Caswell & Vaile \(1995\)](#) and [Caswell \(2003\)](#). We find over these periods that the majority of ex-OH masers have varied, mostly by less than a factor of two. However, twenty-three sources have varied by more than a factor of two. Some of these sources have also changed the direction of variability (increasing to decreasing or vice versa) between the three observing times, suggestive of variation on short timescales.

One important feature of ex-OH masers is their sensitivity to the local magnetic field. A companion paper will present the results of the polarisation data of the ex-OH masers and the derived on the magnetic field strengths ([Avison et al. in prep](#)).

ACKNOWLEDGEMENTS

This work in its initial form was presented as part of LQ's PhD thesis at the University of Manchester ([Quinn 2010](#)) and was revised, re-examined, expanded and completed by AA. The Parkes Observatory and the ATCA are part of the Australia Telescope which is funded by the Commonwealth of Australia for operation as a National Facility managed by CSIRO. AA is funded by the STFC at the UK ARC Node. SLB is the recipient of an Australian Research Council DECRA Fellowship (project number DE130101270) and a L'Oréal-UNESCO for Women in Science Fellowship.

REFERENCES

- Aguirre J. E., et al., 2011, *ApJS*, **192**, 4
- Argon A. L., Reid M. J., Menten K. M., 2000, *ApJS*, **129**, 159
- Baudry A., Desmurs J. F., Wilson T. L., Cohen R. J., 1997, *A&A*, **325**, 255
- Becker R. H., White R. L., Helfand D. J., Zoonematkermani S., 1994, *ApJS*, **91**, 347
- Breen S. L., Ellingsen S. P., Caswell J. L., Lewis B. E., 2010a, *Monthly Notices Royal Astronomical Society*, **401**, 2219
- Breen S. L., Caswell J. L., Ellingsen S. P., Phillips C. J., 2010b, *MNRAS*, **406**, 1487
- Breen S. L., Ellingsen S. P., Contreras Y., Green J. A., Caswell J. L., Stevens J. B., Dawson J. R., Voronkov M. A., 2013, *MNRAS*, **435**, 524
- Breen S. L., et al., 2015, *MNRAS*, **450**, 4109
- Caswell J. L., 1997, *MNRAS*, **289**, 203
- Caswell J. L., 1998, *MNRAS*, **297**, 215

Source Name MMBOH-	S_{MMB} Peak [Jy]	MMB/CV95 Variation factor	S_{MMB} Peak [Jy]	MMB/C03 Variation factor
G000.666−0.029	9.08(R)	0.48	9.08(R)	0.72
G011.034+0.062	2.18(L)	4.54	2.18(L)	1.28
G011.904−0.141	9.87(R)	1.54	9.87(R)	2.47
G015.035−0.677	14.58(R)	0.52	16.68(L)	0.40
G019.486+0.151	1.98(R)	4.13	1.81(L)	0.75
G035.025+0.350	6.09(R)	0.40	6.09(R)	0.74
G035.198−0.743	3.91(L)	3.99	3.91(L)	2.44
G035.200−1.736	0.50(R)	0.15	0.43(L)	0.12
G049.486−0.389	2.05(R)	0.45	2.05(R)	2.56
G284.351−0.418	2.44(R)	0.39	1.97(L)	0.49
G285.263−0.050	<0.74	0.12	-	-
G316.762−0.012	<0.25	0.45	-	-
G330.953−0.182	1.35(R)	1.78	6.67(L)	3.15
G331.542−0.066	22.58(R)	2.75	11.08(L)	1.68
G337.606−0.052	1.18(R)	0.15	0.36(L)	0.16
G338.075+0.012	<0.34	0.40	-	-
G338.280+0.542	<0.33	0.10	-	-
G339.884−1.259	-	-	74.85(R)	2.20
G343.929+0.125	2.45(L)	0.35	2.45(L)	0.82
G345.010+1.792	2.00(L)	0.5	2.00(L)	0.19
G345.003−0.224	5.51(R)	0.32	6.45(L)	1.34
G345.487+0.314	5.17(L)	4.24	5.17(L)	0.78
G348.550−0.979	<0.33	0.18	<0.33	0.33

Table 4. Table of sources which have increased or decreased by a factor of $\geq \pm 2$ or more. Negative values show a decrease in flux density between epochs and positive an increase. For each epoch the polarisation handedness is denoted with R or L in parenthesis in the two MMB column, highlighting which those sources where the handedness has changed. For tentative or non-detected MMB sources the upper limit value is given and only variability between epochs where the previous detection was above this upper limit is listed.

- Caswell J. L., 2001, *MNRAS*, **326**, 805
Caswell J. L., 2003, *MNRAS*, **341**, 551
Caswell J. L., Vaile R. A., 1995, *MNRAS*, **273**, 328
Caswell J. L., et al., 2010, *MNRAS*, **404**, 1029
Caswell J. L., et al., 2011, *MNRAS*, **417**, 1964
Cesaroni R., Walmsley C. M., 1991, *A&A*, **241**, 537
Chen H.-R., et al., 2007, *ApJ*, **654**, L87
Contreras Y., et al., 2013, *A&A*, **549**, A45
Cragg D. M., Sobolev A. M., Ellingsen S. P., Caswell J. L., Godfrey P. D., Sali S. V., Dodson R. G., 2001, *MNRAS*, **323**, 939
Cragg D. M., Sobolev A. M., Godfrey P. D., 2002, *MNRAS*, **331**, 521
Cyganowski C. J., et al., 2008, *AJ*, **136**, 2391
Dame T. M., Thaddeus P., 2008, *ApJ*, **683**, L143
Desmurs J. F., Baudry A., 1998, *A&A*, **340**, 521
Desmurs J.-F., Baudry A., Sivagnanam P., Henkel C., Richards A. M. S., Bains I., 2010, *A&A*, **520**, A45
Ellingsen S., Voronkov M., Cragg D., Sobolov A., Breen S., Godfrey P., 2007, in *Astrophysical masers and their environments*.
Fish V. L., 2007, in *Chapman J. M., Baan W. A., eds, IAU Symposium Vol. 242, IAU Symposium*. pp 71–80
([arXiv:0704.0242](https://arxiv.org/abs/0704.0242)), doi:10.1017/S1743921307012604
Fish V. L., Reid M. J., 2006, *ApJS*, **164**, 99
Forster J. R., Caswell J. L., 1989, *A&A*, **213**, 339
Georgelin Y. M., Georgelin Y. P., 1976, *A&A*, **49**, 57
Gray M. D., 2001, *MNRAS*, **324**, 57
Gray M., 2012, *Maser Sources in Astrophysics*. Cambridge University Press
Gray M. D., Field D., Doel R. C., 1992, *A&A*, **262**, 555
Green J. A., McClure-Griffiths N. M., 2011, *MNRAS*, **417**, 2500
Green J. A., et al., 2009, *Monthly Notices Royal Astronomical Society*, **392**, 783
Green J. A., et al., 2010, *MNRAS*, **409**, 913
Green J. A., et al., 2012a, *MNRAS*, **420**, 3108
Green J. A., McClure-Griffiths N. M., Caswell J. L., Robishaw T., Harvey-Smith L., 2012b, *MNRAS*, **425**, 2530
Guzmán A. E., Garay G., Brooks K. J., 2010, *ApJ*, **725**, 734
Guzmán A. E., Garay G., Brooks K. J., Voronkov M. A., 2012, *ApJ*, **753**, 51
Henshaw J. D., et al., 2016, *MNRAS*, **457**, 2675
Hill T., Burton M. G., Minier V., Thompson M. A., Walsh A. J., Hunt-Cunningham M., Garay G., 2005, *MNRAS*, **363**, 405
Hindson L., Thompson M. A., Urquhart J. S., Faimali A., Clark J. S., Davies B., 2012, *MNRAS*, **421**, 3418
Knowles S. H., Caswell J. L., Goss W. M., 1976, *MNRAS*, **175**, 537
Kruijssen J. M. D., Dale J. E., Longmore S. N., 2015, *MNRAS*, **447**, 1059
Kurtz S., 2005, in *Cesaroni R., Felli M., Churchwell E., Walmsley M., eds, IAU Symposium Vol. 227, Massive Star Birth: A Crossroads of Astrophysics*. pp 111–119, doi:10.1017/S1743921305004424
Larson R. B., 2003, *Reports on Progress in Physics*, **66**
Longmore S. N., et al., 2013, *MNRAS*, **433**, L15
Minier V., Ellingsen S. P., Norris R. P., Booth R. S., 2003, *A&A*, **403**, 1095
Mottram J. C., Hoare M. G., Lumsden S. L., Oudmaier R. D., Urquhart J. S., Sheret T. L., Clarke A. J., Allsopp J., 2007a, *A&A*, **476**, 1019
Mottram J. C., Hoare M. G., Lumsden S. L., Oudmaier R. D., Urquhart J. S., Sheret T. L., Clarke A. J., Allsopp J., 2007b, *Astronomy and Astrophysics*, **476**, 1019
Quinn L. J., 2010, PhD thesis, University of Manchester
Reid M. J., et al., 2009, *ApJ*, **700**, 137
Reid M. J., et al., 2014, *ApJ*, **783**, 130
Richards A. M. S., 2012, in *Booth R. S., Vlemmings W. H. T., Humphreys E. M. L., eds, IAU Symposium Vol. 287, Cosmic Masers - from OH to H0*. pp 199–208, doi:10.1017/S1743921312006977

- Rosolowsky E., et al., 2010, [ApJS](#), **188**, 123
- Rydbeck O. E. H., Kollberg E., Elldér J., 1970, [ApJ](#), **161**, L25
- Sánchez-Monge Á., Pandian J. D., Kurtz S., 2011, [ApJ](#), **739**, L9
- Schuller F., et al., 2009, [A&A](#), **504**, 415
- Sutton E. C., Sobolev A. M., Ellingsen S. P., Cragg D. M., Mehringer D. M., Ostrovskii A. B., Godfrey P. D., 2001, [ApJ](#), **554**, 173
- Taylor J. H., Cordes J. M., 1993, [ApJ](#), **411**, 674
- Trinidad M. A., 2011, [AJ](#), **142**, 147
- Urquhart J. S., et al., 2014, [A&A](#), **568**, A41
- Vallée J. P., 2014, [ApJS](#), **215**, 1
- van der Walt J., 2005, [Monthly Notices Royal Astronomical Society](#), **360**, 153
- van der Walt D. J., Goedhart S., Gaylard M. J., 2009, [MNRAS](#), **398**, 961
- Walsh A. J., Burton M. G., Hyland A. R., Robinson G., 1998, [Monthly Notices Royal Astronomical Society](#), **301**, 640
- Wilson W. E., et al., 2011, [MNRAS](#), **416**, 832
- Xu Y., Li J. J., Hachisuka K., Pandian J. D., Menten K. M., Henkel C., 2008, [A&A](#), **485**, 729
- Yen J. L., Zuckerman B., Palmer P., Penfield H., 1969, in *Bulletin of the American Astronomical Society*. p. 269
- Zoonematkermani S., Helfand D. J., Becker R. H., White R. L., Perley R. A., 1990, [ApJS](#), **74**, 181

Table 1: MMB Survey ex-OH Catalogue. Columns 1: Source Name, which is defined as the source position in Galactic coordinates (rounded at the third decimal point). Columns 2 & 3: source position ins Right Ascension and Declination (sources with positions from MMB observations have three decimal places in RA and two in Dec, all previously detected masers have two and one decimal accuracy respectively). Column 4: The ex-OH transition for the listed maser, counterpart 6030-MHz masers are listed directly below their 6035-MHz partner. Column 5: Reference for the position listed, with the following abbreviations ATCA 09, ATCA 13 and ATCA 14 denote our ATCA observation results from 2009, October 2013 and February 2014 respectively observations. C03 = [Caswell \(2003\)](#), C01 = [Caswell \(2001\)](#). Columns 6 to 11: The ex-OH maser peak flux density, velocity of peak and a minimum-maximum velocity range over which emission is seen in the spectrum, first for left hand circular polarisation (LHCP) and then right hand circular polarisation (RHCP). Sources in *italics* are values for Stokes I (total intensity) flux density taken from the respective ATCA observation as these sources are not present in the nearest Parkes MX. As such only columns 7 to 9 are filled in. † Sources *333.136–0.432* and *333.135–0.431* have a blended spectrum preventing a complete velocity range to be estimated from the MX data.

Source Name	Source	Position			MX \backslash (ATCA) LHCP \backslash (Stokes I)			MX RHCP		
MMBOH- <i>Glll.lll±bb.bbb</i>	RA hh:mm:ss	Dec dd:mm:ss.s(s)	Transition [MHz]	Position Ref	S_{peak} [Jy]	V_{peak} [km/s]	V_{range} [km/s]	S_{peak} [Jy]	V_{peak} [km/s]	V_{range} [km/s]
0.666−0.029	17:47:18.64	−28:22:54.6	6035	C03	20.07	72.23	68.5, 73.6	9.08	72.06	68.4, 73.5
			6030	C03	1.50	72.28	70.1, 73.2	2.26	70.24	69.7, 72.8
0.666−0.035	17:47:20.14	−28:23:06.2	6035	C03	2.06	67.58	60.0, 68.0	2.10	67.12	66.6, 67.6
4.682+0.278	17:55:18.808	−24:46:24.97	6035	ATCA 09	0.71	2.01	1.3, 3.1	0.22	2.11	1.3, 3.1
5.885−0.392	18:00:30.36	−24:04:03.1	6035	C03	0.52	10.45	0.1, 16.4	0.63	9.51	−1.0, 16.4
6.882+0.094	18:00:49.375	−22:57:37.80	6035	ATCA 09	5.81	−2.34	−4.1, 0.0	1.16	−2.05	−4.1, −0.5
			6030	ATCA 09	1.22	−2.32	−4.3, −1.6	0.43	−12.62	−3.3, −1.4
8.352+0.478	18:02:31.248	−21:29:33.67	6035	ATCA 13	2.18	0.48	0.1, 1.6	1.07	0.38	−0.1, 1.0
8.669−0.356	18:06:19.01	−21:37:32.7	6035	C03	0.66	39.31	37.8, 41.1	0.58	39.31	38.1, 41.1
9.620+0.194	18:06:14.916	−20:31:39.07	6035	ATCA 09	0.89	6.00	−1.7, 8.7	0.59	6.09	−1.2, 7.9
9.622+0.196	18:06:14.639	−20:31:27.67	6035	ATCA 09	0.24	−0.60	−1.0, 0.6	0.25	0.08	−0.8, 0.6
10.322−0.258	18:09:23.307	−20:08:02.20	6035	ATCA 09	0.75	36.59	34.2, 41.0	1.15	35.62	34.2, 38.0
10.623−0.384	18:10:28.65	−19:55:49.6	6035	C03	0.48	−0.60	−5.6, 3.7	0.57	−0.69	−4.8, 3.2
			6030	C03	0.32	0.80	−2.0, 3.4	0.33	0.21	−2.1, 2.4
10.960+0.022	18:09:39.673	−19:26:23.00	6035	ATCA 13	1.50	25.12	23.5, 26.9	3.02	24.73	23.6, 25.5
11.034+0.062	18:09:39.85	−19:21:20.1	6035	C03	2.18	24.05	21.3, 25.7	1.31	23.27	21, 25.3
11.904−0.141	18:12:11.44	−18:41:29.0	6035	C03	1.64	42.88	41.1, 43.3	9.87	42.97	41.1, 43.9
			6030	C03	0.27	42.01	41.4, 44.1	0.26	42.99	42.1, 43.8
12.681−0.182	18:13:54.771	−18:01:43.70	6035	ATCA 09	0.83	58.82	56.4, 61.2	0.52	59.21	56.9, 61.0
15.035−0.677	18:20:24.81	−16:11:34.1	6035	C03	16.68	21.52	20.9, 24.1	14.58	21.52	21.0, 23.7
			6030	C03	2.87	21.64	21.3, 22.2	1.01	21.64	21.1, 22.4
18.460−0.005	18:24:36.400	−12:51:09.89	6035	ATCA 09	0.37	43.88	43.0, 52.2	0.52	43.49	42.9, 52.5
18.836−0.299	18:26:23.681	−12:39:30.80	6035	ATCA 09	0.35	41.69	41.1, 43.8	0.60	41.50	40.5, 43.3
19.486+0.151	18:26:00.39	−11:52:21.9	6035	C03	1.81	25.41	24.4, 26.1	1.98	25.41	24.0, 26.7
			6030	C03	0.58	25.45	24.7, 26.0	0.51	25.45	25.0, 26.0
19.752−0.191	18:27:44.910	−11:47:49.94	6035	PIGGY	0.37	117.84	115.7, 119.1	0.29	116.39	114.6, 119.1
20.237+0.065	18:27:44.56	−11:14:54.6	6035	C03	2.51	71.51	71.0, 73.1	2.59	71.51	70.1, 74.5
			6030	C03	0.37	71.44	71.2, 71.8	0.39	71.54	71.2, 71.8
24.147−0.010	18:35:21.020	−07:48:58.99	6035	ATCA 09	0.27	17.42	16.1, 18.2	6.67	17.42	15.8, 18.3
25.648+1.050	18:34:20.575	−05:59:45.40	6035	ATCA 13	2.50	39.58	38.7, 40.3	0.72	38.71	38.2, 40.0
25.509−0.060	18:38:03.249	−06:37:46.90	6035	ATCA 09	1.04	95.50	92.3, 97.1	1.20	95.40	91.8, 97.8
28.200−0.049	18:42:58.07	−04:13:57.0	6035	C03	5.48	96.08	92.9, 100.0	3.50	96.27	92, 101.0
			6030	C03	0.63	96.29	90.1, 99.4	1.15	95.02	92.8, 98.9
28.819+0.366	18:42:37.335	−03:29:34.57	6035	ATCA 14	0.60	88.38	87.3, 90.8	0.27	88.00	86.9, 91.8

continued ...

Source Name	Source	Position				MX/(ATCA) LHCP /(Stokes I)			MX RHCP		
MMBOH- <i>Glll.lll±bb.bbb</i>	RA hh:mm:ss	Dec dd:mm:ss.s(s)	Transition [MHz]	Position Ref	S_{peak} [Jy]	V_{peak} [km/s]	V_{range} [km/s]	S_{peak} [Jy]	V_{peak} [km/s]	V_{range} [km/s]	
30.778−0.801	18:50:21.583	−02:16:55.00	6035	ATCA 09	0.52	77.24	77.3, 78.4	1.22	77.62	77.0, 78.2	
32.744−0.076	18:51:21.88	−00:12:05.5	6035	C03	0.47	33.95	29.3, 39.7	0.91	33.66	29.3, 41.7	
34.258+0.153	18:53:18.68	+01:15:00.3	6035	C03	0.46	58.19	54.7, 63.2	0.71	58.48	51.7, 63.8	
34.258+0.153b	18:53:18.68	+01:15:00.0	6035	C03, ATCA 09	3.95	54.31	55.1, 63.1	2.67	54.50	54.0, 56.4	
			6030	C03	2.20	54.34	53.7, 54.9	0.48	54.64	54.2, 56.3	
34.261−0.213	18:54:37.360	+01:05:08.60	6035	ATCA 09	0.62	58.45	53.9, 54.9	0.71	58.35	54.3, 55.4	
35.025+0.350	18:54:00.66	+02:01:19.3	6035	C03	3.25	45.32	44.8, 45.8	6.09	45.61	45.1, 46.1	
35.133−0.744	18:58:06.146	+01:37:09.50	6035	ATCA 13	2.24	35.80	34.9, 36.6	0.98	36.48	35.2, 36.8	
35.198−0.743	18:58:13.06	+01:40:37.7	6035	C03	3.91	30.46	29.9, 30.7	—	—	—, —	
35.200−1.736	19:01:45.55	+01:13:33.3	6035	C01, C03	0.43	44.34	40.2, 45.7	0.50	42.98	39.1, 45.3	
40.282−0.220	19:05:41.209	+06:26:11.80	6035	ATCA 14	0.86	73.88	73.5, 74.3	0.23	74.56	74, 74.7	
40.426+0.701	19:02:39.62	+06:59:12.0	6035	C01, C03	0.29	14.48	10.0, 18.5	0.49	16.04	9.6, 18.5	
43.149+0.013	19:10:11.05	+09:05:22.1	6035	C01, C03	3.65	11.16	9.0, 14.4	3.38	10.86	7.9, 13.2	
43.165+0.013	19:10:12.85	+09:06:12.0	6035	C01, C03	1.56	13.19	16.6, 18.3	1.21	13.09	16.0, 18.3	
			6030	C03	0.40	13.49	16.7, 18.1	0.20	13.39	16.7, 18.1	
43.796−0.127	19:11:53.97	+09:35:51.8	6035	C01, C03	0.54	40.29	37.7, 44.9	0.59	40.29	38.2, 45.4	
45.123+0.133	19:13:27.80	+10:53:39.1	6035	C01, C03	1.79	67.51	66.4, 70.9	4.06	67.60	65.3, 71.3	
45.466+0.045	19:14:25.66	+11:09:26.5	6035	C01, C03	10.25	66.38	62.4, 69.5	7.48	64.93	62.1, 69.3	
			6030	C03	1.73	65.23	64.1, 68.2	1.64	64.84	64.2, 68.7	
48.988−0.300	19:22:26.035	+14:06:30.99	6035	ATCA 09	1.65	67.53	66.3, 71.2	3.58	67.63	65.4, 71.0	
<i>49.046−0.290</i>	<i>19:22:30.778</i>	<i>+14:09:52.59</i>	<i>6035</i>	<i>ATCA 09</i>	<i>1.21</i>	<i>67.97</i>	<i>66.5, 72.1</i>				
49.490−0.388	19:23:43.93	+14:30:34.9	6035	C01, C03	6.29	57.40	50.8, 60.5	6.98	57.70	51.1, 65.5	
			6030	C01, C03	—	—	—, —	1.59	52.69	51.4, 55.1	
49.486−0.389	19:23:43.85	+14:30:29.9	6035	C01, C03	1.99	55.10	54.3, 56.1	2.05	55.80	54.5, 56.5	
50.478+0.705	19:21:40.286	+15:53:46.39	6035	ATCA 09	4.80	48.12	47.4, 48.9	0.82	48.22	47.1, 48.8	
51.681+0.714	19:24:00.392	+16:57:39.400	6035	ATCA 14	0.31	7.14	5.1, 8.6	0.45	7.04	5.7, 8.0	
189.030+0.783	—	—	6035	MX only, see §3	0.6	3.36	2.2, 4.5	0.98	3.27	2.3, 4.3	
240.316+0.071	07:44:51.97	−24:07:42.3	6035	CV95, C03	2.64	63.62	62.2, 64.3	0.95	63.62	61.7, 64.3	
284.016−0.856	10:20:16.299	−58:03:50.20	6035	ATCA 09	0.60	14.25	12.5, 15.9	1.62	14.05	13.3, 15.5	
284.351−0.418	10:24:10.68	−57:52:34.0	6035	C03	1.97	5.86	5.1, 8.9	2.44	5.76	1.1, 12.5	
			6030	C03	1.73	5.87	4.3, 9.5	2.00	5.78	3.6, 8.8	
294.511−1.621	11:35:32.21	−63:14:43.0	6035	C03	5.44	−11.99	−12.3, −11.6	4.71	−11.99	−12.3, −11.6	
298.723−0.086	12:14:39.674	−62:39:23.10	6035	ATCA 09	0.28	24.84	24.6, 25.2	0.20	24.06	23.9, 24.5	
300.969+1.148	12:34:53.27	−61:39:39.9	6035	C03	17.10	−37.39	−39.2, −35.3	12.08	−37.58	−39.4, −35.4	
			6030	C03	10.09	−37.17	−37.7, −36.8	5.39	−37.66	−38.1, −37.2	
305.200+0.019	13:11:16.90	−62:45:54.7	6035	C03	1.70	−31.37	−37.7, −30.4	3.31	−31.56	−38.6, −30.0	
305.208+0.206	13:11:13.800	−62:34:41.1	6035	ATCA 13	0.98	−34.90	−35.1, −34.2	1.25	−35.39	−35.6, −35.1	
305.362+0.150	13:12:35.933	−62:37:17.30	6035	ATCA 09	0.41	−36.05	−36.5, −35.3	0.36	−35.76	−36.8, −35.0	
308.056−0.396	13:36:32.327	−62:49:05.20	6035	ATCA 09	15.93	−14.11	−15.3, −9.8	25.46	−13.62	−16.0, −10.5	
308.651−0.507	13:41:50.399	−62:49:04.90	6035	ATCA 09	0.35	2.27	1.2, 4.4	0.42	2.17	1.4, 4.2	
309.384−0.135	13:47:24.192	−62:18:11.80	6035	ATCA 09	0.51	−51.37	−52.9, −47.9	2.25	−52.05	−53.4, −49.7	
309.901+0.231	13:51:00.966	−61:49:54.79	6035	ATCA 09	0.56	−55.16	−55.8, −54.1	0.73	−55.16	−56.0, −54.0	
309.921+0.479	13:50:41.77	−61:35:10.1	6035	C01, C03	20.20	−59.43	−62.4, −57.3	18.84	−61.56	−62.8, −57.2	
			6030	C03	3.62	−58.05	−62.6, −56.9	3.11	−59.32	−62.7, −57.2	
311.596−0.398	14:06:18.35	−62:00:15.3	6035	C03	1.82	29.74	28.8, 32	1.61	30.61	27.9, 32.4	

continued ...

Source Name	Source	Position			MX/(ATCA) LHCP /(Stokes I)			MX RHCP		
MMBOH- <i>Glll.lll±bb.bbb</i>	RA hh:mm:ss	Dec dd:mm:ss.s(s)	Transition [MHz]	Position Ref	S_{peak} [Jy]	V_{peak} [km/s]	V_{range} [km/s]	S_{peak} [Jy]	V_{peak} [km/s]	V_{range} [km/s]
311.643−0.380	14:06:38.74	−61:58:23.1	6035	C03	1.15	33.91	28.6, 35.2	0.71	30.61	27.7, 35.7
312.598+0.045	14:13:14.958	−61:16:53.90	6035	ATCA 09	0.51	−66.72	−68.7, −62.1	0.66	−66.33	−67.9, −65.8
320.427+0.103	15:09:39.787	−57:59:40.68	6035	ATCA 09	0.60	−14.05	−15.0, −12.5	0.25	−13.66	−15.3, −12.4
323.459−0.079	15:29:19.332	−56:31:21.26	6035	C97	27.14	−70.50	−70.9, −65.4	44.18	−70.21	−70.7, −65.4
			6030	C03	1.69	−70.39	−64.0, −71.5	1.69	−70.19	−65.0, −70.7
<i>326.447−0.749</i>	<i>15:49:18.525</i>	<i>−55:16:56.98</i>	<i>6035</i>	<i>ATCA 09</i>	0.55	<i>−60.92</i>	<i>−61.7, −60.2</i>			
326.448−0.749	15:49:18.701	−55:16:53.98	6035	ATCA 09	0.92	−60.88	−61.8, −59.7	1.82	−60.78	−62.2, −59.7
			6030	ATCA 09	0.57	−60.76	−59.9, −61.4	0.80	−60.57	−60.0, −61.3
327.944−0.116	15:54:34.002	−53:50:47.90	6035	ATCA 09	0.57	−52.05	−52.6, −51.3	0.65	−51.95	−52.4, −51.6
328.236−0.548	15:57:58.348	−53:59:25.20	6035	C03, ATCA 09	1.35	−44.21	−47.4, −36.4	0.52	−46.05	−48.1, −35.7
			6030	C03, ATCA 09	0.38	−45.73	−46.2, −45.4	0.41	−46.04	−46.4, −45.7
328.307+0.430	15:54:06.44	−53:11:41.1	6035	C98, C03	3.39	−90.52	−95.5, −88.9	2.96	−90.33	−94.2, −89.2
328.808+0.633	15:55:48.39	−52:43:06.7	6035	C03	22.76	−46.08	−47.1, −42.3	13.70	−45.79	−47.3, −42.1
329.031−0.197	16:00:30.38	−53:12:25.5	6035	C98	0.21	−38.77	−39.0, −37.5	0.17	−32.46	−32.8, −32
329.184−0.314	16:01:47.103	−53:11:40.60	6035	ATCA 09	0.24	−55.48	−57.7, −53.3	0.19	−55.68	−56.3, −54.6
329.339+0.148	16:00:33.15	−52:44:39.8	6035	C03	0.63	−104.72	−107.8, −103.5	0.81	−104.04	−107.3, −103.2
329.405−0.459	16:03:32.15	−53:09:29.9	6035	C03	0.33	−70.47	−71.4, −67.2	0.17	−70.36	−71.3, −69.8
330.953−0.182	16:09:52.38	−51:54:57.6	6035	C03	6.67	−87.82	−90.2, −86.7	1.35	−88.01	−90.5, −86.7
331.512−0.102	16:12:09.856	−51:28:35.86	6035	ATCA 09, C03	2.97	−89.86	−93.0, −88.4	2.82	−89.04	−93.0, −88.4
			6030	C03	0.26	−89.39	−90.7, −88.6	0.24	−89.10	−90.2, −88.6
331.512−0.102	16:12:10.049	−51:28:34.96	6035	ATCA 09, C03	2.68	−86.83	−88.0, −84.3	5.40	−85.98	−88.0, −84.3
331.543−0.066	16:12:09.137	−51:25:45.43	6035	ATCA 09, C03	11.08	−85.98	−94.0, −84.6	22.58	−85.89	−87.9, −84.7
332.824−0.548	16:20:10.758	−50:53:18.1	6035	ATCA 13	1.14	−54.98	−58.4, −53.7	2.49	−54.69	−57.7, −54.0
332.964−0.679	16:21:23.057	−50:52:56.49	6035	ATCA 09	0.21	−48.26	−48.6, −47.9	0.15	−48.36	−48.6, −47.9
333.068−0.447	16:20:49.096	−50:38:38.87	6035	ATCA 09	0.74	−56.10	−56.2, −55.7	0.38	−55.90	−56.2, −55.7
333.136−0.432	16:21:03.112	−50:35:08.70	6035	ATCA 09/ C03	7.79	−50.24	†, −47.8	7.32	−50.43	†, −47.8
333.135−0.431	16:21:02.92	−50:35:10.0	6035	C03	10.31	−51.21	−59.9, †	10.76	−51.40	−59.9, †
			6030	C03	1.47	−51.10	−61.2, −48.9	1.51	−51.10	−61.2, −48.9
333.228−0.055	16:19:47.960	−50:15:11.50	6035	ATCA 09	0.23	−88.87	−92.1, −87.7	0.26	−90.13	−91.2, −87.7
333.608−0.215	16:22:11.162	−50:05:56.75	6035	C03	2.17	−51.61	−59.0, −41.9	1.55	47.63	−52.5, −50.8
336.822+0.028	16:34:38.29	−47:36:32.9	6035	C01	1.17	−77.13	−79.1, −75.0	1.13	−77.52	−78.7, −76.8
336.941−0.156	16:35:55.20	−47:38:45.8	6035	C03	4.19	−65.39	−71.2, −64.5	1.52	−64.90	−71.2, −63.6
			6030	C03	2.38	−65.27	−69.5, −68.1	0.40	−64.89	−68.1, −63.7
336.983−0.183	16:36:12.39	−47:37:57.8	6035	C03	0.56	−65.70	−66.6, −63.5	0.28	−65.12	−66.3, −63.9
337.098−0.928	16:39:58.012	−48:02:44.399	6035	ATCA 13	0.64	−42.10	−39.1, −37.8	0.21	−42.01	−42.3, −41.7
337.404−0.402	16:38:50.45	−47:28:03.2	6035	C03	1.56	−35.51	−42.2, −35.0	1.14	−35.22	−42.2, −34.7
			6030	C03	0.46	−35.50	−36.3, −35.2	0.41	−35.01	−36.3, −34.6
337.606−0.052	16:38:09.54	−47:04:59.9	6035	C03	0.36	−42.21	−50.3, −37.3	0.38	−42.41	−43.8, −40.1
337.705−0.053	16:38:29.67	−47:00:35.8	6035	C03	1.65	−51.13	−55.7, −46.3	2.90	−50.65	−56.5, −46.4
			6030	C03	0.35	−49.66	−55.8, −44.7	0.31	−48.50	−55.5, −46.7
337.844−0.374	16:40:26.716	−47:07:12.25	6035	ATCA 09	0.93	−37.75	−39.8, −36.9	2.17	−37.95	−39.7, −37.5
338.925+0.557	16:40:33.53	−45:41:37.2	6035	C03	0.47	−62.80	−64.5, −57.0	0.28	−62.80	−64.5, −57.5
339.053−0.315	16:44:48.99	−46:10:13.1	6035	C03	0.23	−110.90	−112.2, −110.1	0.24	−111.28	−112.5, −110.6
339.282+0.136	16:43:43.12	−45:42:08.0	6035	C03	0.59	−70.87	−73.0, −66.0	0.76	−71.07	−73.4, −66.2
339.622−0.121	16:46:05.96	−45:36:44.1	6035	C03	0.96	−30.17	−34.7, −28.9	1.90	−30.47	−34.7, −29.4

continued ...

Source Name	Source	Position				MX/(ATCA) LHCP /(Stokes I)			MX RHCP		
MMBOH- <i>Glll.lll±bb.bbb</i>	RA hh:mm:ss	Dec dd:mm:ss.s(s)	Transition [MHz]	Position Ref	S_{peak} [Jy]	V_{peak} [km/s]	V_{range} [km/s]	S_{peak} [Jy]	V_{peak} [km/s]	V_{range} [km/s]	
339.884−1.259	16:52:04.61	−46:08:34.0	6035	C01, C03	68.48	−37.36	−38.3, −36.6	74.85	−37.36	−38.5, −36.9	
			6030	C01, C03	42.14	−37.15	−38.4, −36.0	46.51	−37.44	−38.6, −35.7	
339.980−0.539	16:49:14.949	−45:36:31.13	6035	ATCA 09	1.81	−88.68	−89.3, −88.5	1.12	−88.97	−89.3, −88.7	
340.785−0.096	16:50:14.84	−44:42:26.7	6035	C03	5.93	−102.07	−106.3, −100.1	6.20	−101.88	−107.0, −100.1	
341.974+0.225	16:53:05.355	−43:35:09.69	6035	ATCA 09	0.74	−6.02	−8.7, −4.0	0.32	−4.66	−112.5, −110.6	
343.354−0.067	16:59:04.452	−42:41:34.39	6035	ATCA 09	0.52	−116.89	−118.5, −115.9	1.09	−117.09	−118.2, −116.4	
343.929+0.125	17:00:10.91	−42:07:19.3	6035	C03	2.45	13.67	11.5, 16.2	1.49	14.06	12.0, 15.6	
344.419+0.044	17:02:08.60	−41:47:10.2	6035	C03	0.73	−63.26	−65.0, −62.8	0.45	−62.97	−65.0, −62.5	
345.010+1.792	16:56:47.58	−40:14:25.7	6035	C03	2.00	−21.38	−23.6, −14.8	1.16	−17.69	−24.0, −14.8	
			6030	C03	0.79	−20.58	−22.5, −18.9	0.85	−20.29	−22.3, −18.9	
345.003−0.224	17:05:11.20	−41:29:07.0	6035	C03	6.45	−25.95	−31.1, −24.2	5.51	−25.75	−31.7, −24.4	
345.407−0.951	17:09:35.40	−41:35:55.0	6035	C03	0.82	−26.66	−27.0, −25.5	0.80	−26.27	−26.8, −25.8	
345.487+0.314	17:04:28.12	−40:46:25.3	6035	C01, C03	5.17	−22.05	−22.6, −21.5	2.57	−22.15	−22.6, −21.5	
			6030	C01, C03	1.00	−22.03	−23.2, −21.1	0.44	−21.84	−23.4, −21.1	
345.495+1.469	16:59:41.741	−40:03:39.70	6035	ATCA 09	0.48	−12.51	−19.5, −9.4	0.55	−12.31	−19.5, −10.5	
345.698−0.090	17:06:50.60	−40:50:59.6	6035	C03	8.44	−6.45	−9.2, −1.9	8.58	−6.45	−7.0, −3.0	
			6030	C03	3.17	−4.88	−7.3, −2.4	2.72	−4.78	−6.6, −2.7	
347.628+0.149	17:11:50.89	−39:09:29.0	6035	C03	5.41	−96.87	−97.5, −94.1	11.92	−96.48	−97.8, −94.7	
			6030	C03	2.00	−96.85	−97.6, −96.5	3.15	−96.57	−97.1, −96.1	
348.698−1.027	17:19:58.98	−38:58:13.5	6035	C03	2.58	−14.61	−17.1, −13.1	0.56	−15.87	−16.8, −13.3	
350.014+0.434	17:17:45	−37:03:12.9	6035	C98	0.29	−35.43	−36.0, −31.5	0.31	−35.62	−37.0, −31.4	
350.113+0.095	17:19:25.58	−37:10:04.4	6035	C03	0.38	−72.06	−72.6, −70.5	0.45	−72.25	−72.7, −70.7	
350.686−0.491	17:23:28.63	−37:01:48.1	6035	C03	1.58	−13.64	−15.9, −13.3	2.11	−13.83	−16.3, −13.3	
351.417+0.645	17:20:53.37	−35:47:01.2	6035	C03	333.07	−10.25	−11.2, −6.9	253.32	−10.45	−11.5, −7.3	
			6030	C03	39.21	−10.24	−11.1, −6.1	26.66	−10.63	−11.5, −7.2	
351.581−0.353	17:25:25.08	−36:12:46.1	6035	C03	7.98	−96.41	−101.3, −89.8	3.65	−96.31	−101.3, −89.5	
			6030	C03	0.66	−96.00	−103.9, −91.6	0.78	−96.30	−103.9, −91.6	
351.775−0.536	17:26:42.56	−36:09:16.0	6035	C03	2.31	−7.44	−9.5, −2.3	4.40	−7.64	−9.0, −2.4	
353.410−0.360	17:30:26.18	−34:41:46.0	6035	C03	25.48	−20.65	−22.4, −17.5	16.56	−20.75	−22.9, −17.5	
			6030	C03	3.74	−21.61	−22.7, −20.3	4.00	−22.29	−23.2, −21.7	
354.725+0.299	17:31:15.831	−33:14:04.70	6035	C03, ATCA 09	0.97	91.76	88.7, 95	0.89	90.20	88.7, 94.7	
355.344+0.147	17:33:29.05	−32:47:58.8	6035	C03	5.08	18.11	17.4, 19.6	5.00	17.81	17.1, 18.9	
			6030	C03	2.81	18.22	16.8, 19.8	3.13	17.83	16.8, 19.2	
357.924−0.338	17:41:55.472	−30:52:50.77	6035	ATCA 09	0.73	−3.57	−4.0, −3.0	0.91	−3.57	−4.0, −3.2	
359.137+0.031	17:43:25.64	−29:39:18.3	6035	C03	2.93	−1.93	−3.3, 0.9	2.58	−1.93	−3.8, 0.5	

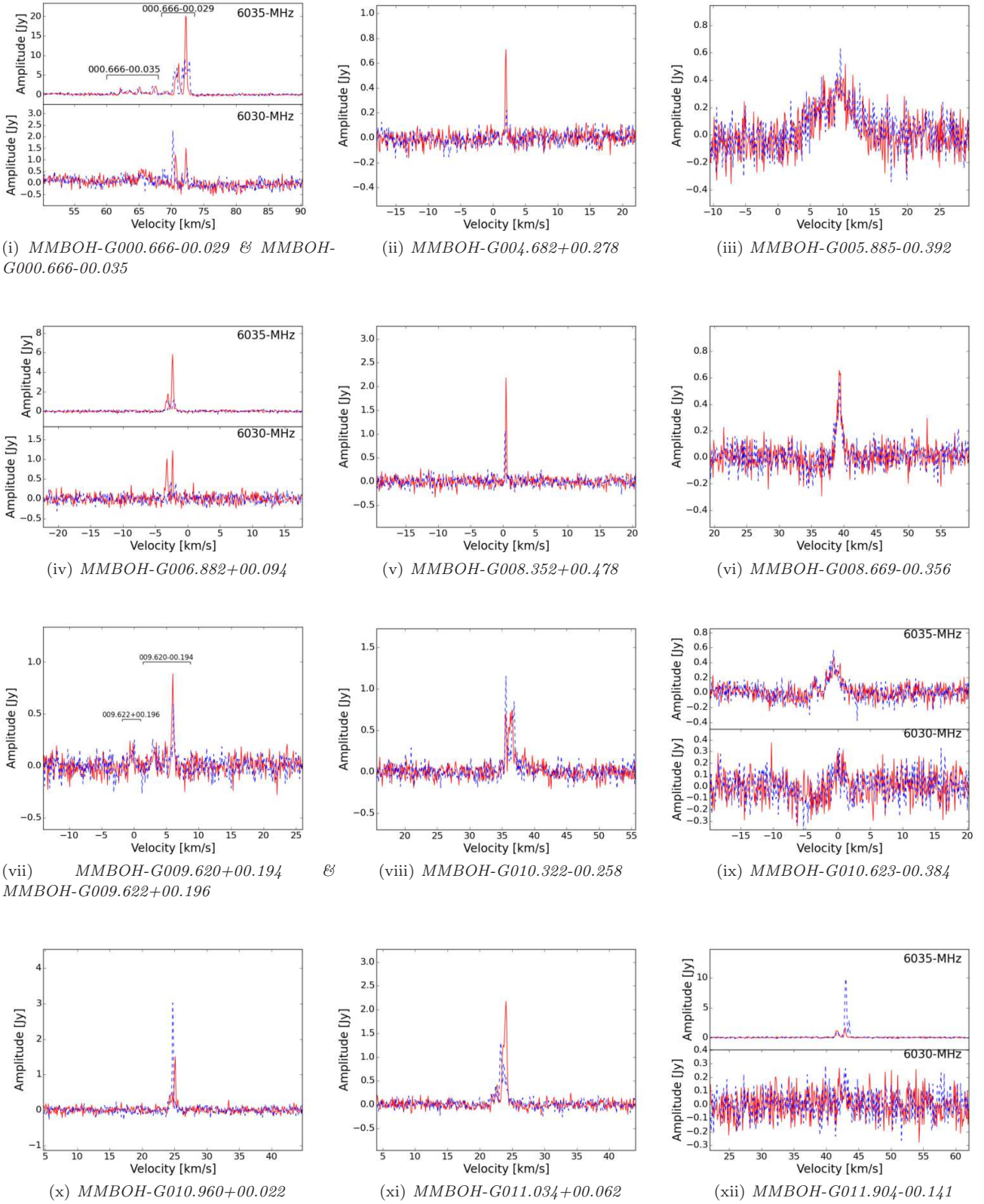


Figure 11. MMB ex-OH maser spectra from the Parkes ‘MX’ observations. Red (solid) and blue (dashed) lines are right and left hand circular polarisations respectively. Spectra for two sources are presented ($49.046-0.290$ and $326.447-0.749$) in black (dash-dot) lines, these are Stokes I spectra from ATCA as these sources are not present in the nearest Parkes MX. The full version of this figure is available in the online version of this paper.

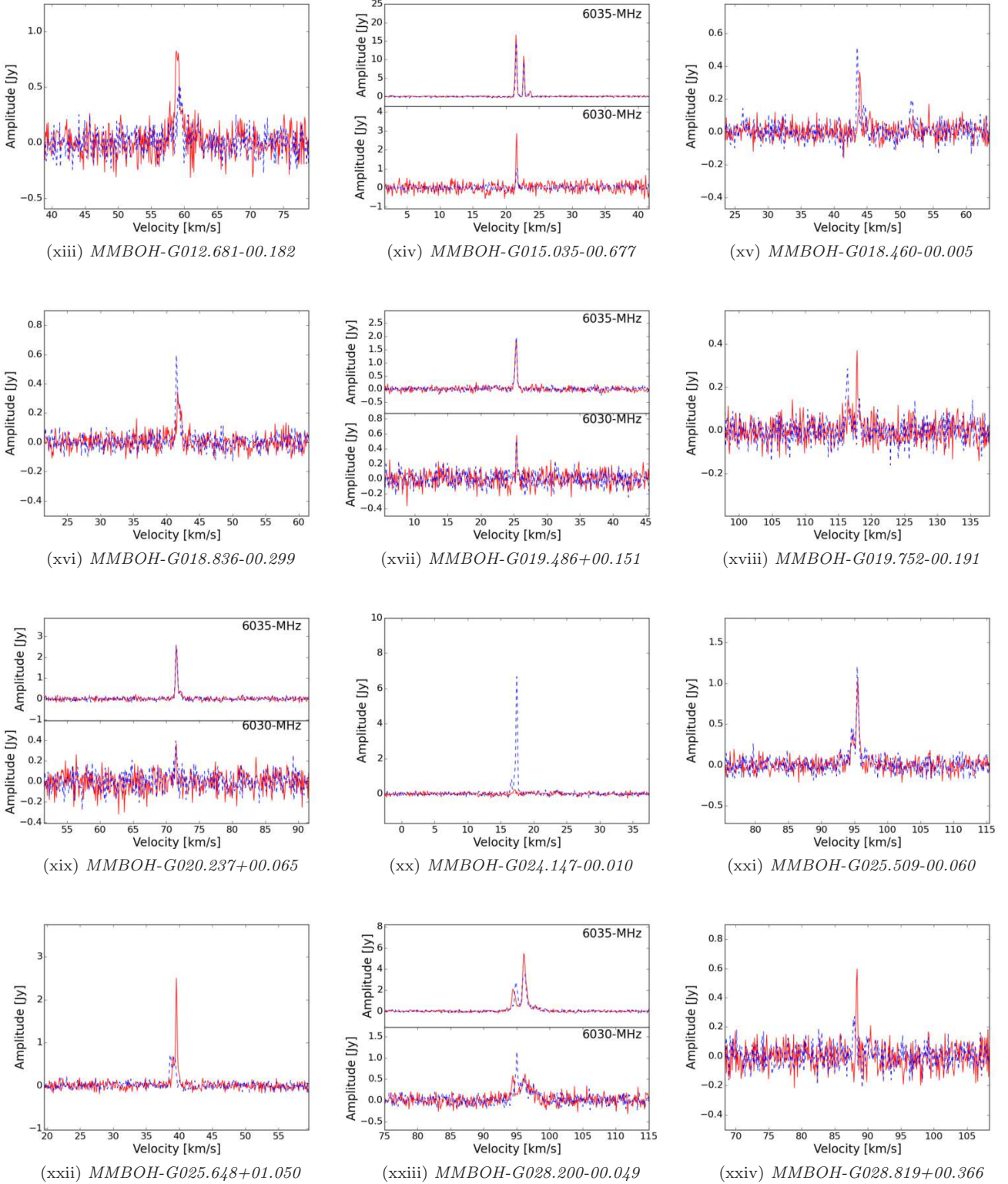


Figure 11. (continued)

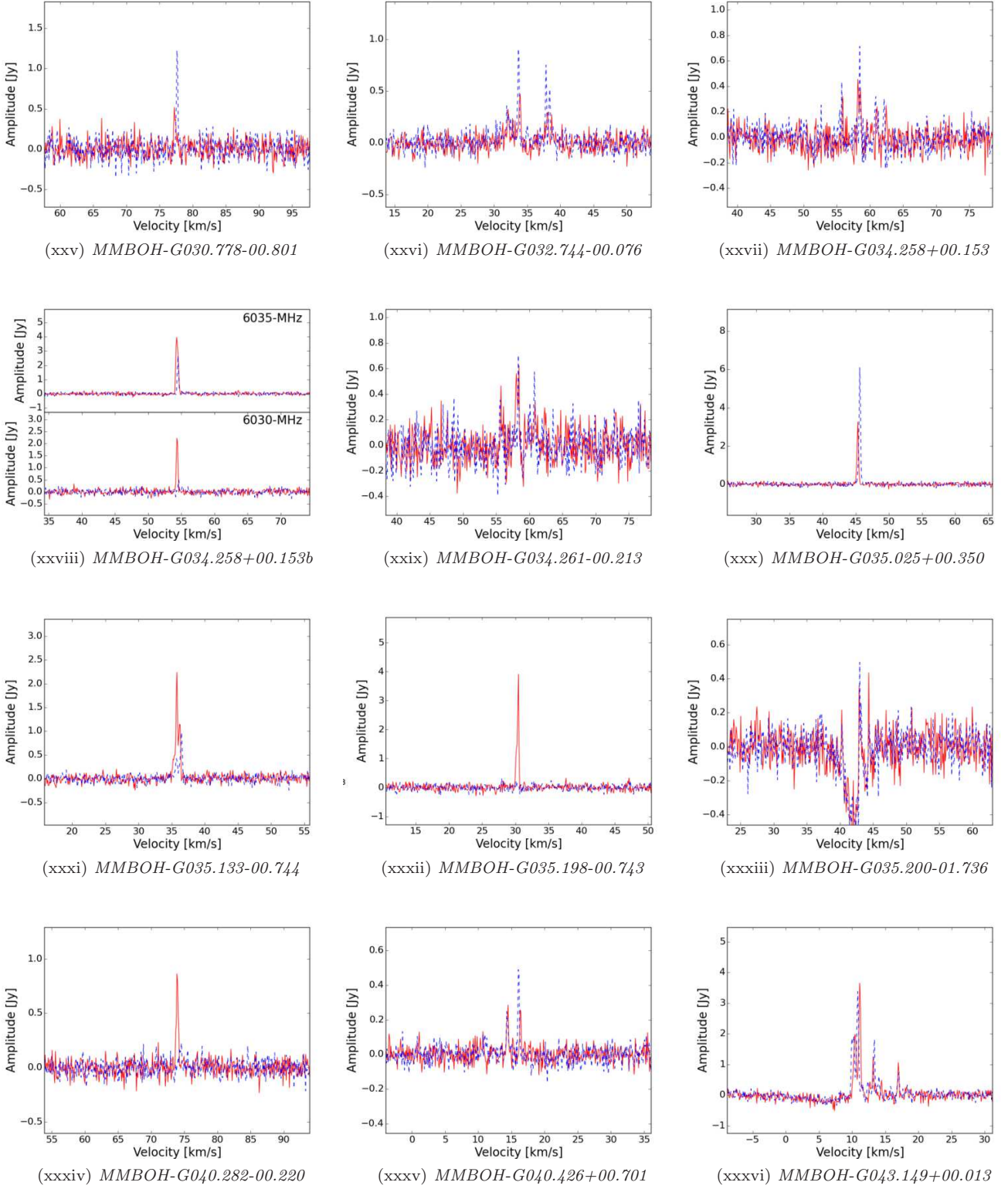


Figure 11. (continued)

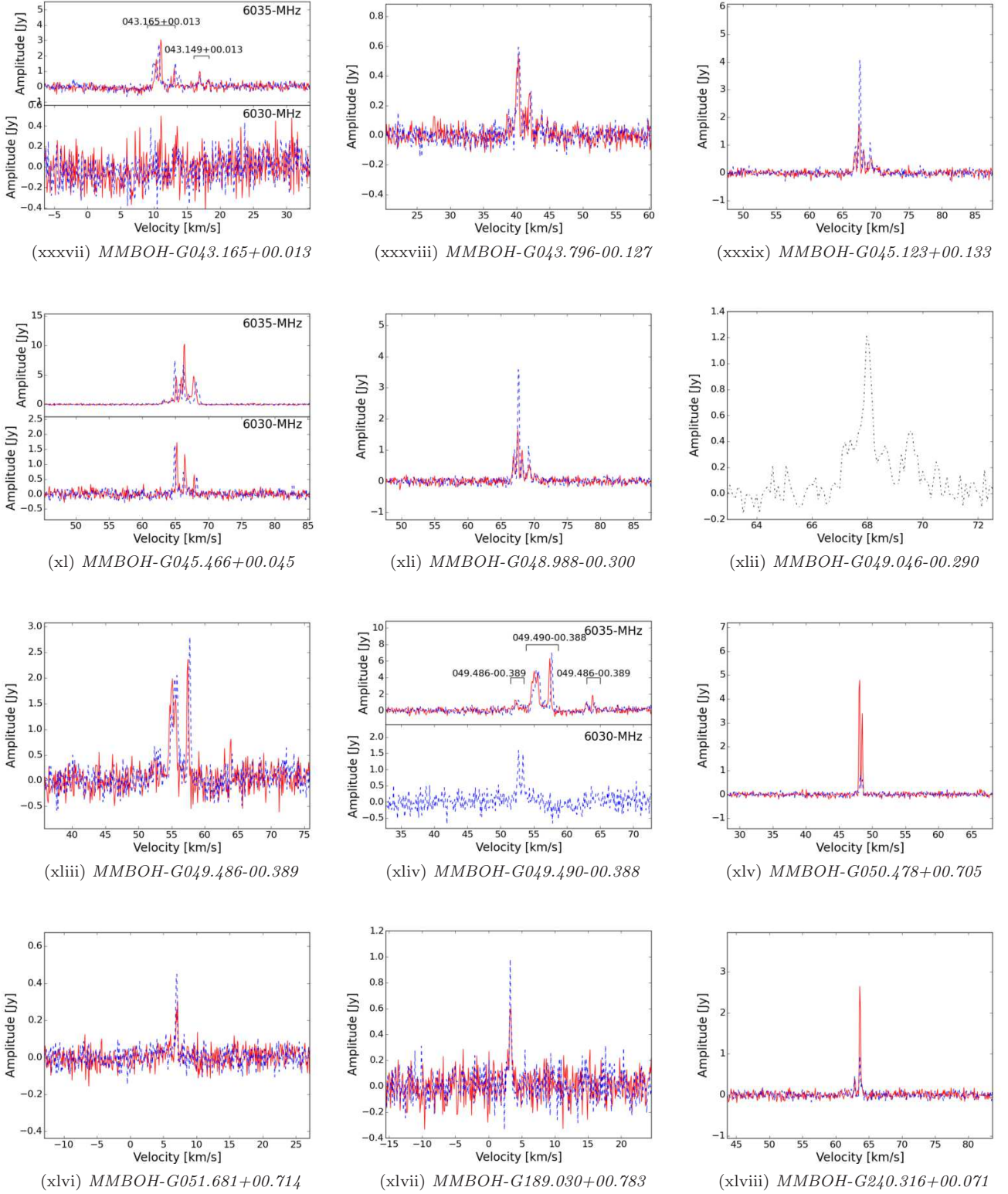


Figure 11. (continued)

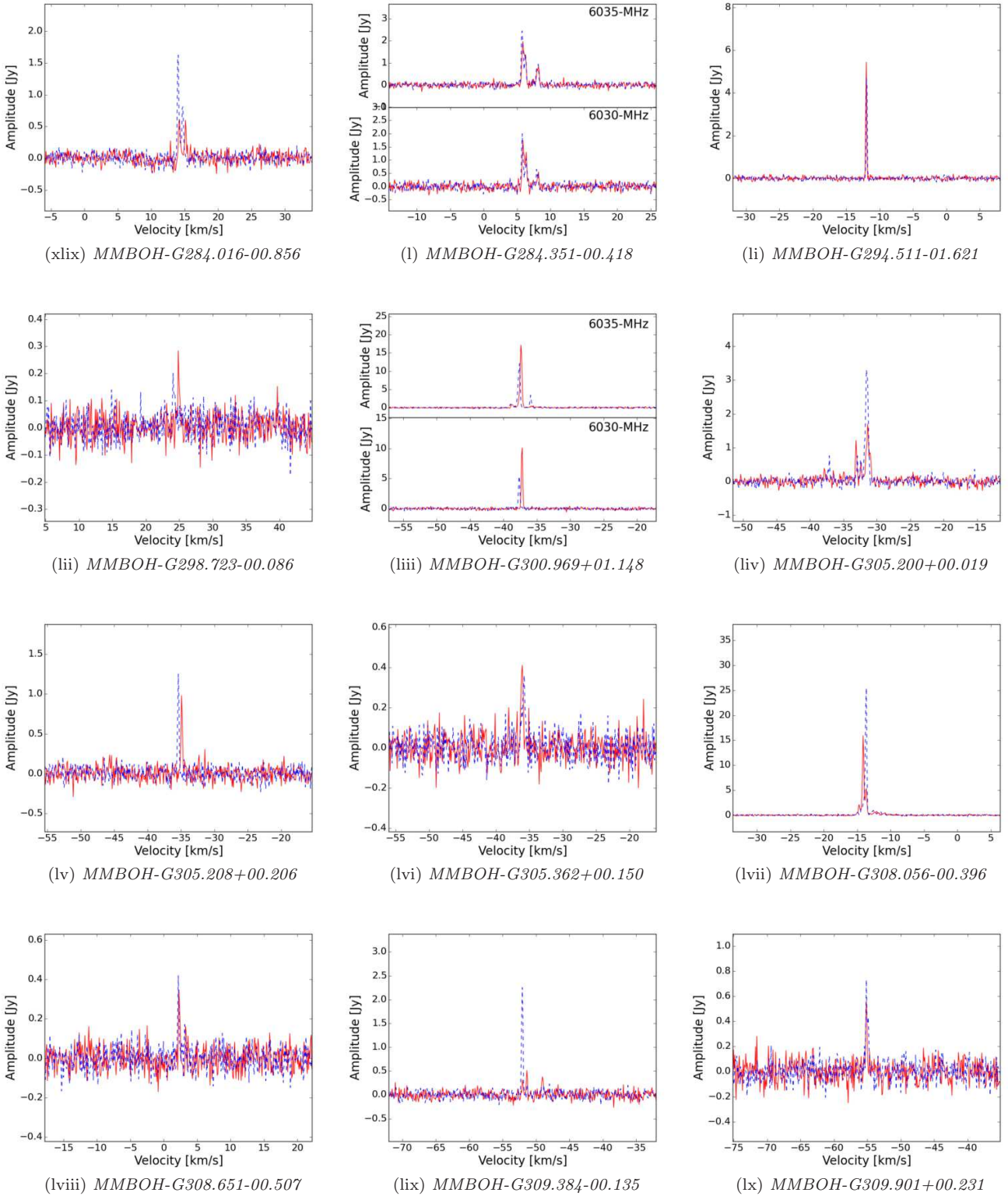


Figure 11. (continued)

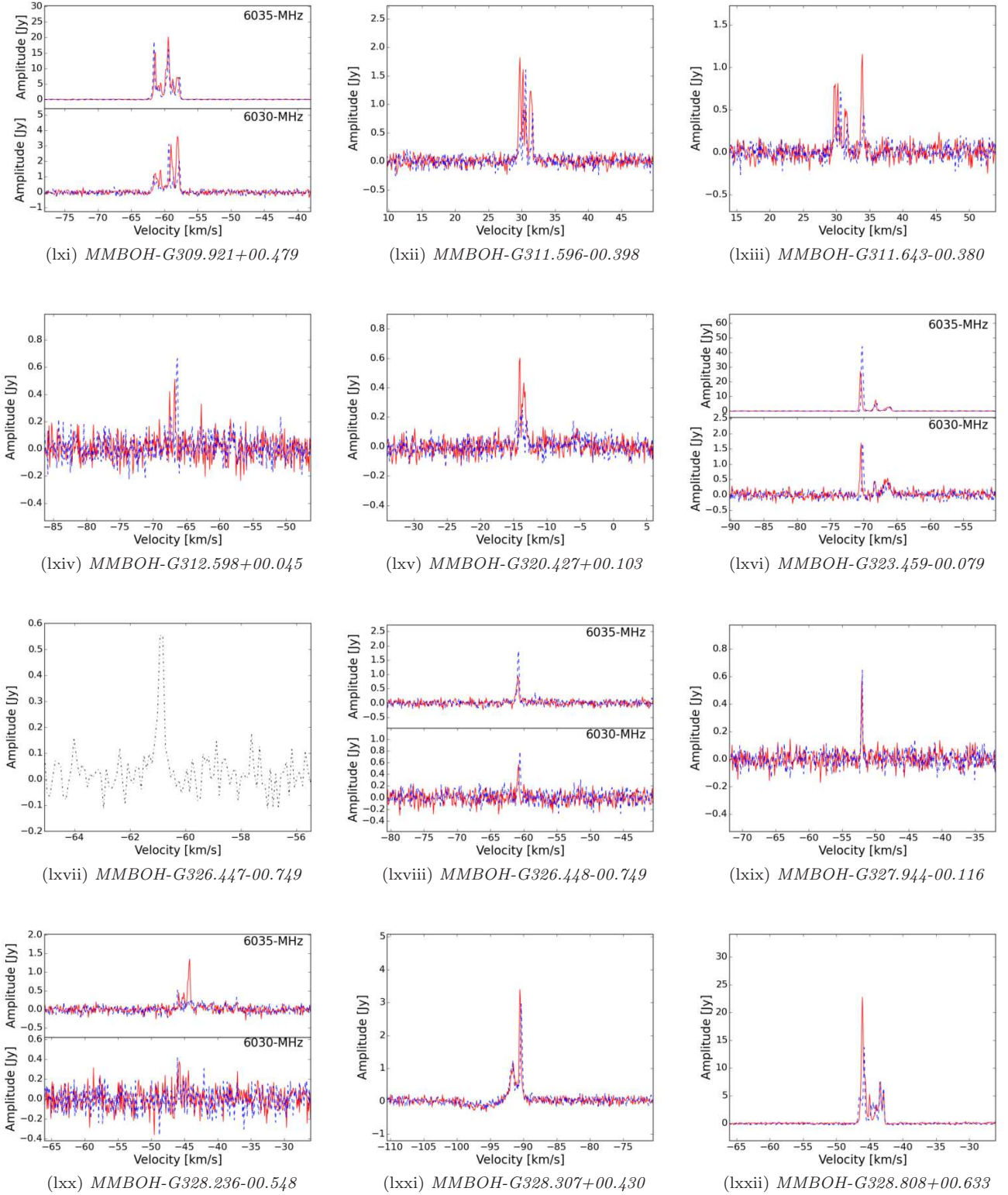


Figure 11. (continued)

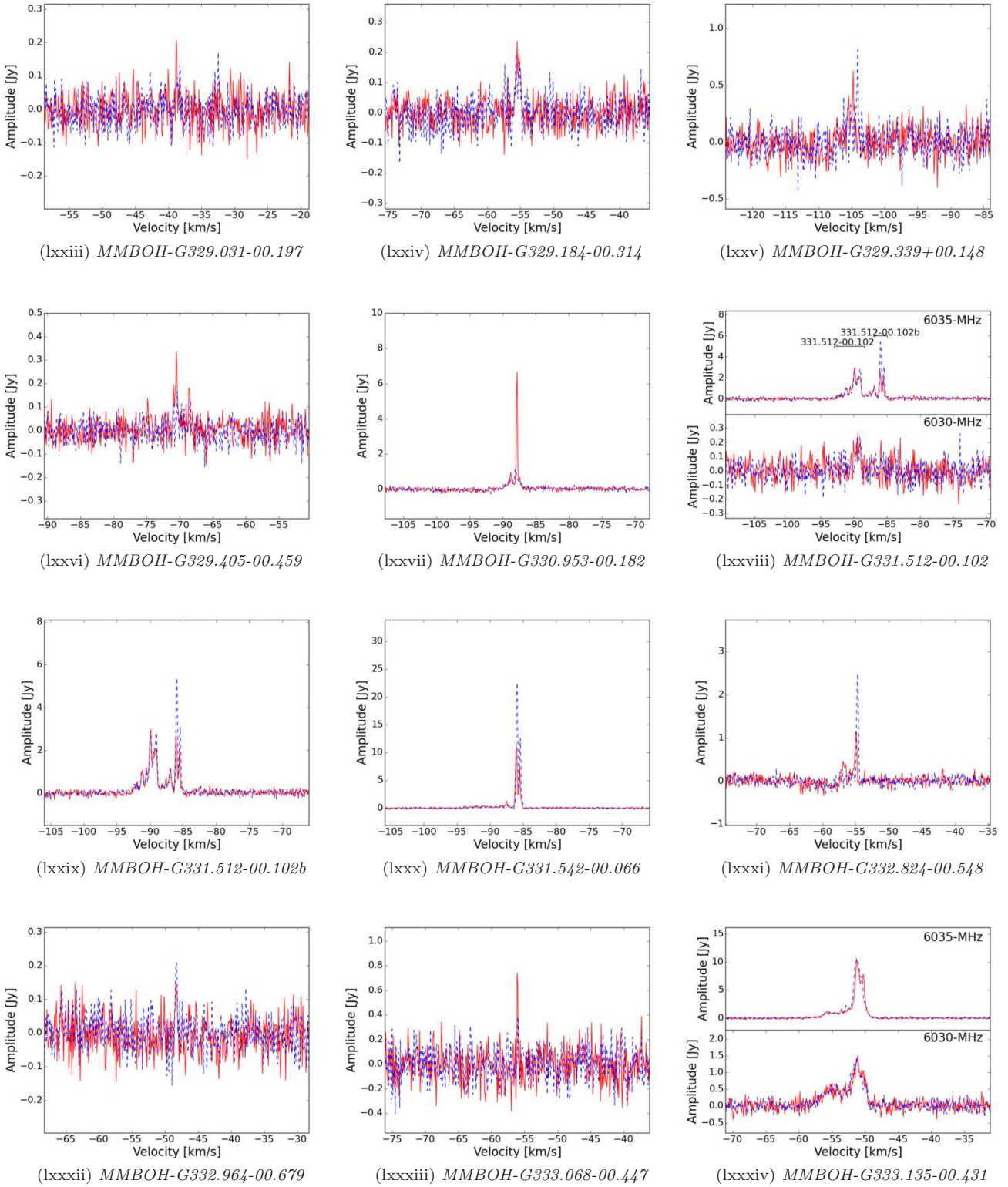


Figure 11. (continued)

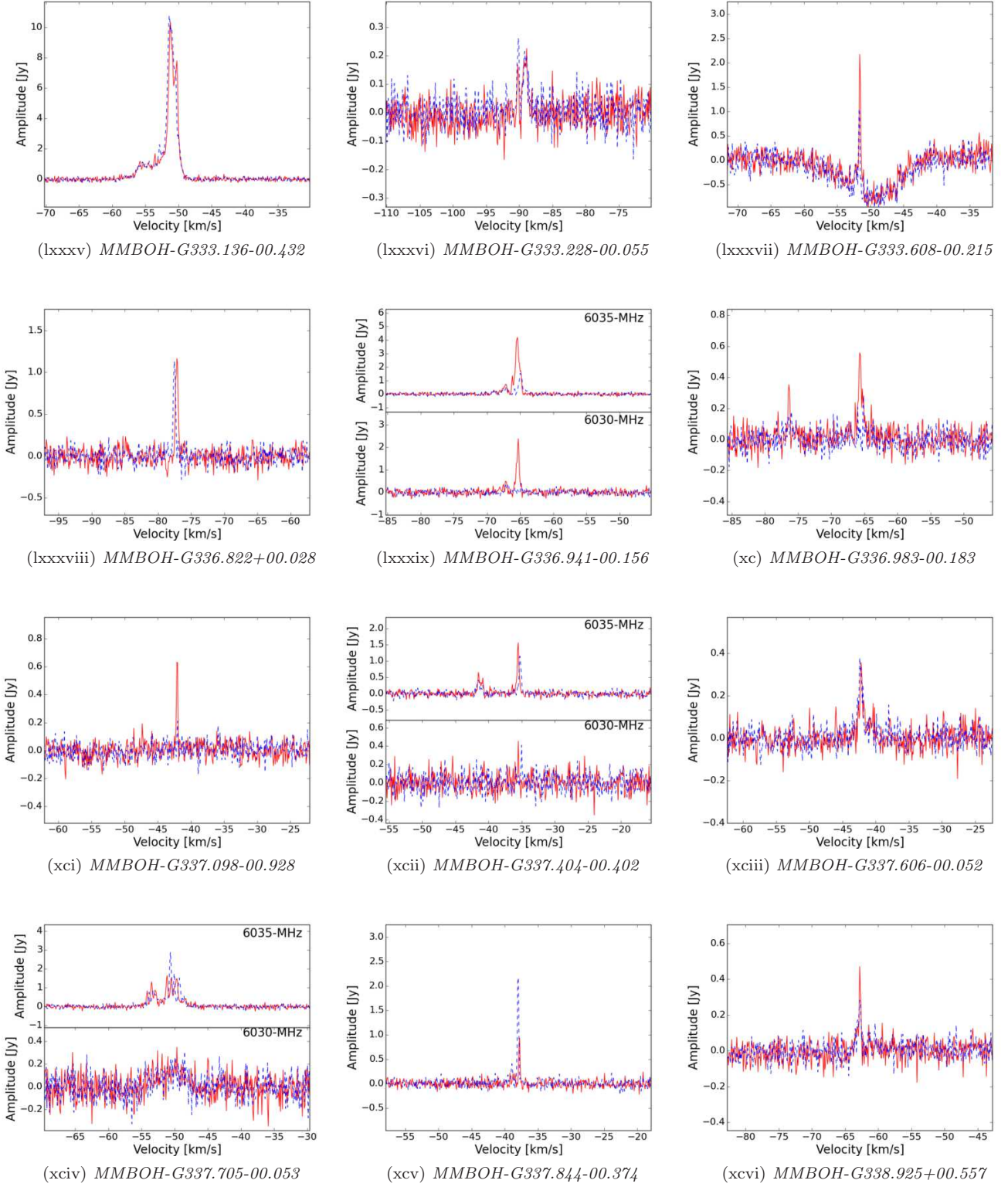


Figure 11. (continued)

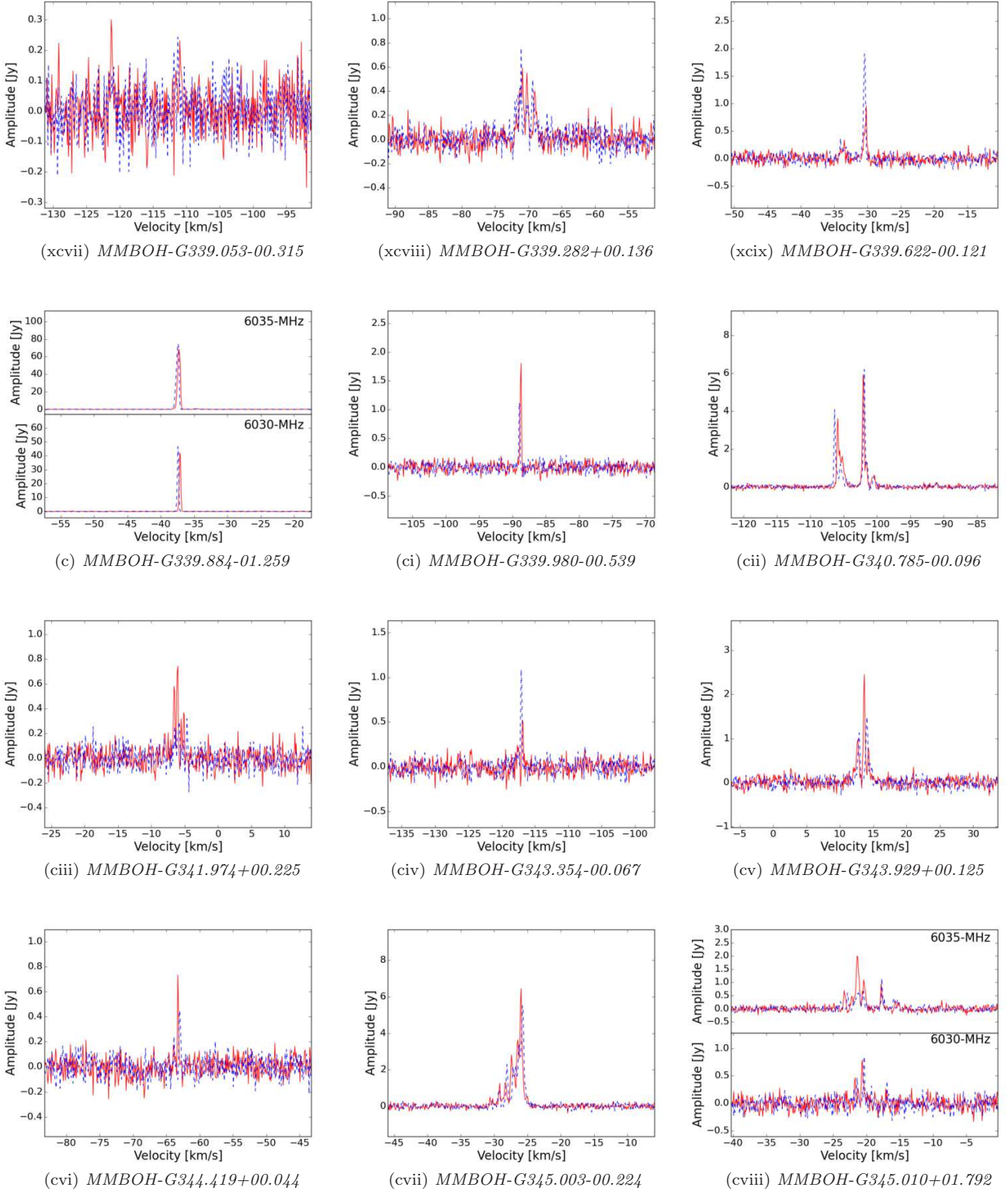


Figure 11. (continued)

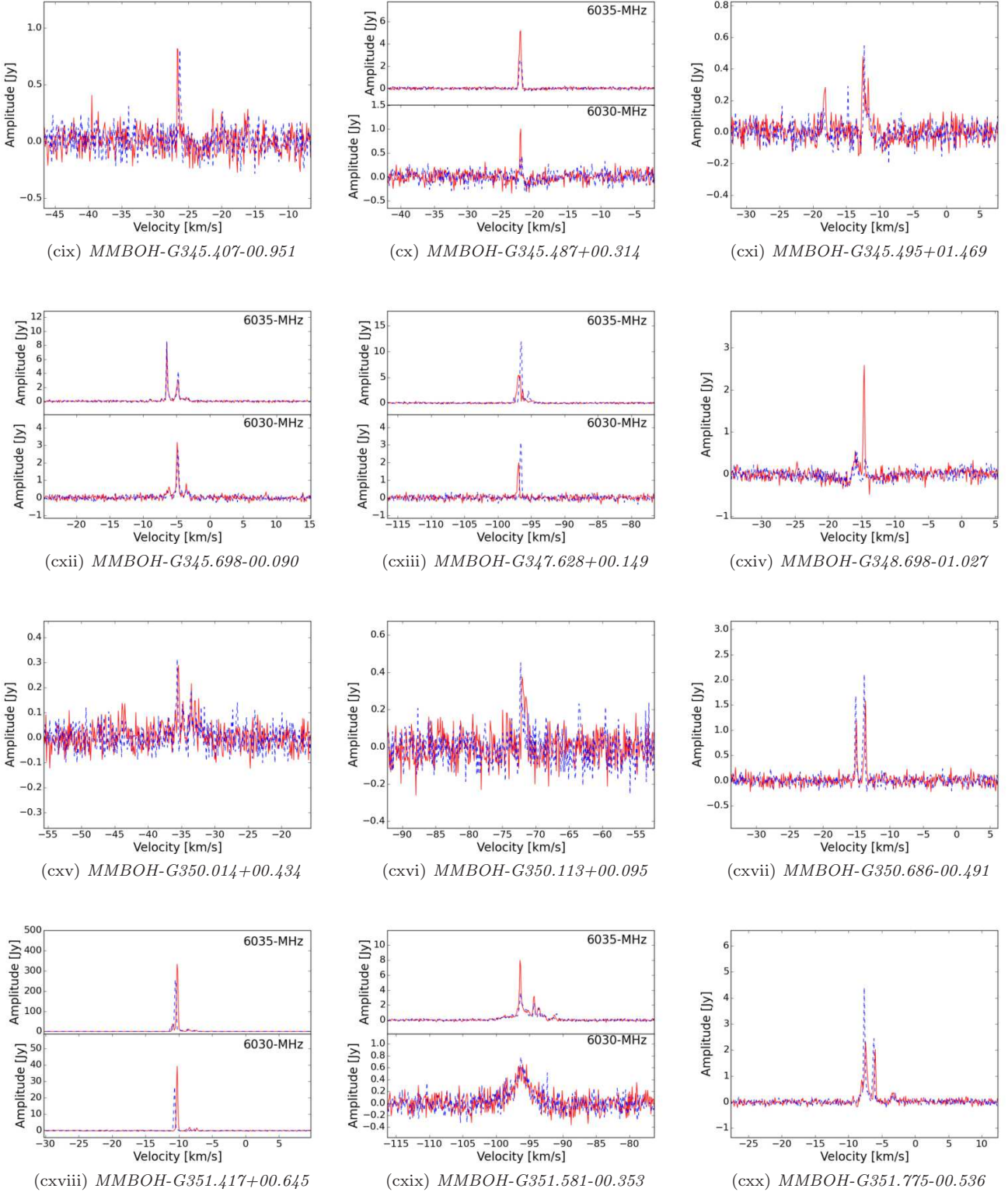


Figure 11. (continued)

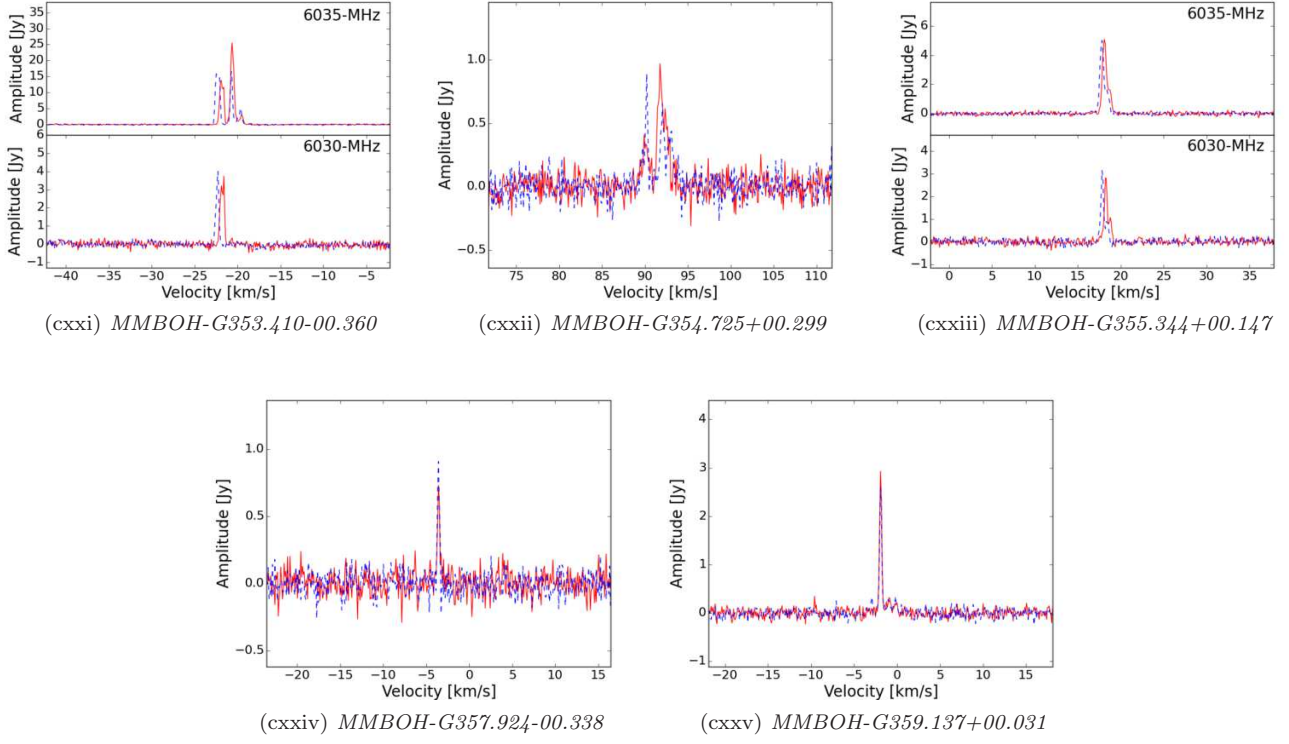


Figure 11. (continued)